Relative strength of the pyrope-majorite solid solution and the flow-law of majorite containing garnets

Simon A. Hunt, David P. Dobson, Li Li, Donald J. Weidner, John P. Brodholt

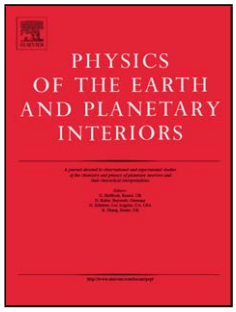

Title: Relative strength of the pyrope–majorite solid solution and the flow-law of majorite containing garnets

Authors: Simon A. Hunt, David P. Dobson, Li Li, Donald J. Weidner, John P. Brodholt

PII: S0031-9201(09)00240-4
DOI: doi:10.1016/j.pepi.2009.12.001
Reference: PEPI 5229

To appear in: *Physics of the Earth and Planetary Interiors*

Received date: 11-5-2009
Revised date: 26-11-2009
Accepted date: 7-12-2009

Please cite this article as: Hunt, S.A., Dobson, D.P., Li, L., Weidner, D.J., Brodholt, J.P., Relative strength of the pyrope–majorite solid solution and the flow-law of majorite containing garnets, *Physics of the Earth and Planetary Interiors* (2008), doi:10.1016/j.pepi.2009.12.001

Relative strength of the pyrope–majorite solid solution and the flow-law of majorite containing garnets.

Simon A. Hunt*[,a,b], David P. Dobson[a], Li Li[c], Donald J. Weidner[c], John P. Brodholt[a]

[a] *Department of Earth Sciences, University College London, Gower Street, London. WC1E 6BT, UK*
[b] *Department of Chemistry, University College London, 20 Gordon Street, London. WC1H 0AJ, UK*
[c] *SUNY Stony Brook, Inst. Mineral. Phys., Dept. Geosci., Stony Brook, NY 11790 USA*

Abstract

Even though the garnet phase is the second most abundant phase in the upper-mantle and transition-zone, no previous studies have directly measured the effect of majorite content on the strength of garnet under mantle conditions. Here we report the results of constant strain-rate and stress-relaxation experiments on garnets in the pyrope–majorite solid solution which constrain the strength of majoritic containing garnets relative to pyrope as a function of majorite content and temperature. We find that at temperatures below 650 °C both pure pyrope and majoritic garnets have the same strength. Conversely, above 650 °C we find that majoritic garnets are initially stronger than pure pyrope but weaken with increasing temperature and majorite content and with significant majorite contents are weaker than pyrope above approximately 800 °C. We develop a flow law for the entire pyrope–majorite solid solution as a function of temperature and majorite content.

Key words: garnets, transition-zone, majorite rheology, flow-law, high-pressure, high-temperature

1. Introduction

The garnet phase is the second most abundant mineral component of the upper mantle and transition zone, after olivine and its high pressure polymorphs. In undifferentiated pyrolite mantle, the modal amount of garnet is about 15 % at depths of 100–300 km increasing to around 40 % between 500 and 600 km. In subducting slabs the percentage garnet in the MORB component of the slab can be as high as 90 % between depths of 450 and 550 km (Ringwood 1991). There is potential, therefore, for the garnet phase to have a significant influence on mantle dynamics. However, despite this there have been, to date, relatively few studies measuring the rheology of even pure pyrope, let alone other garnet compositions relevant to the mantle. Studies that have been undertaken measuring the flow of pyrope include Wang and Shaocheng (2000), Dobson et al. (2005) and Li et al. (2006).

The increasing amount of garnet with depth in the subducting slab and mantle is the result of the increased solubility of pyroxene (generically $AB(Si_2O_6)$, where A and B are the two cations) in garnet as the pressure and temperature increase. This changes the composition of the pyrope ($Mg_3Al_2Si_3O_{12}$)-rich garnet to give an increasing majorite ($Mg_4Si_4O_{12}$) content, by substituting Mg^{2+} and Si^{4+} onto the

*Corresponding author: s.hunt@ucl.ac.uk

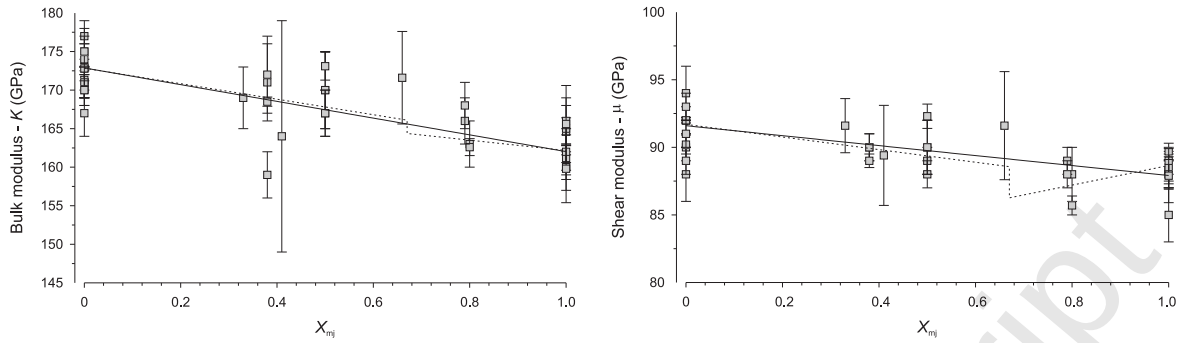

(a) Bulk modulus – K **(b)** Shear modulus – μ

Figure 1: Plot of K and μ values reported in the literature for the pyrope–majorite solid solution (updated after Sinogeikin et al. 1997), where $X_{\mathrm{mj}} = [\mathrm{mj}]/([\mathrm{mj}] + [\mathrm{py}])$. The solid lines are the weighted fit to all the data for which there are published errors and the dotted lines are the separate weighted fits to the data with majorite contents above and below 67 %, after the preferred fit of Sinogeikin et al. (1997). The coefficients for the solid and both parts of the dashed lines are presented in table 1. The data are taken from: Sato et al. (1978), Leitner et al. (1980), Sumino and Anderson (1984), Duffy and Anderson (1989), Bass and Kanzaki (1990), Leger et al. (1990), Yeganeh-Haeri et al. (1990), O'Neill et al. (1991), Armbruster et al. (1992), Rigden et al. (1994), Pacalo and Weidner (1997), Sinogeikin et al. (1997), Gwanmesia et al. (1998), Wang et al. (1998), Chen et al. (1999), Conrad et al. (1999), Zhang et al. (1999), Gwanmesia et al. (2000), Lui et al. (2000), Wang and Ji (2001), Sinogeikin and Bass (2002a,b), Gwanmesia et al. (2006).

octahedral site, which is occupied by Al^{3+} in pyrope. As the majorite content of the garnet increases there is a corresponding decrease in the bulk and shear modulae (figures 1a and b).

Various authors (e.g. Cohen 1991, Gilman 2003) have argued that a material's bulk modulus is a good guide to its resistance to plastic deformation. Assuming that this is applicable in the garnet solid solution, majorite-rich garnets should be mechanically weaker than pyrope. The opposite conclusion is drawn by Karato et al. (1995) who argued that the strength of a range of low-pressure garnet-structured materials is a function of homologous temperature and normalised creep strength; they argue that majorite garnet should follow the same trend and will therefore be stronger than pyrope in the transition zone. Kavner et al. (2000) find that majorite supports a larger shear stress than pyrope in room temperature diamond-anvil cell studies, consistent with the conclusions of Karato et al. (1995); however, no high temperature studies of majorite strength or rheology have previously been reported.

We have performed relative-strength experiments to resolve the conundrum as to whether majoritic garnets are stronger or weaker than pyrope, as well as to generate sufficient data to calculate a flow law for more majorite-rich garnets. The relative strength experiments were undertaken on beam line X17B2 at the NSLS, Brookhaven National Laboratory, USA.

2. Experimental method

The relative-strength experiments reported here were performed on beamline X17B2 at the NSLS (Weidner et al. 1992), using both the Deformation-DIA (D-DIA; Wang et al. 2003) and T-Cup (Vaughan et al. 1998) multi-anvil press modules in a 200 tonne load frame. The detector arrangement of this beamline consisted of four energy-dispersive detectors aligned in pairs to observe the diffraction patterns

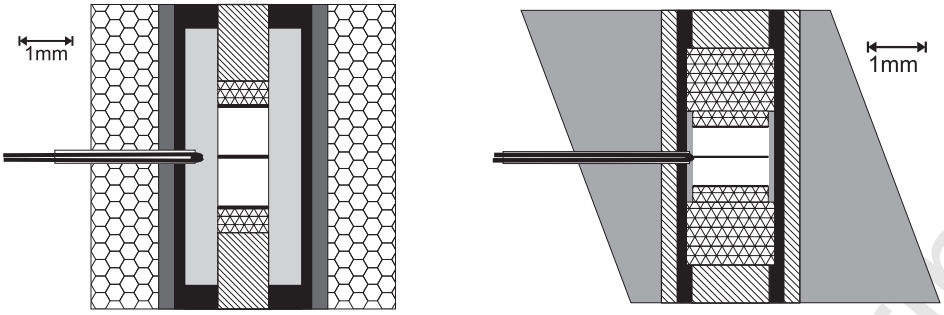

(a) 6/4 D-DIA cell **(b)** 7/3 T-Cup cell

Figure 2: A schematic of the D-DIA cell and a example of the T-Cup cell used at the NSLS in this study. The hexagons are the boron epoxy cube for the D-DIA cell, the dark grey – MgO, black – graphite, light grey – boron nitride, triangles – Al_2O_3 pistons, hatching – crushable alumina, heavy black lines are foil markers between the samples which are white.

from the samples both parallel and perpendicular to the direction of uniaxial deformation. This is sufficient to constrain the hydrostatic and differential stress on the sample because the sample geometry is axi-symmetric. The diffraction detectors are complimented by a fluorescent YAG crystal and visible light CCD camera which image the sample during the experiment. Each experiment contained two samples which were stacked on top of each other and then deformed simultaneously under near-identical conditions; such an experimental design has been used previously (e.g. Li et al. 2003, 2006, Hunt et al. 2009).

The first experiment in this study was performed in a 6/4 D-DIA cell to investigate the relative strength of pyrope and $py_{95}mj_5$ as a function of temperature; the cell design for this experiment is illustrated in figure 2a. This was followed by experiments in the T-Cup to investigate the relative strength of more majoritic garnets (which would exolve enstatite at the lower pressures attainable in the D-DIA) and pyrope in stress relaxation experiments. The T-Cup experiments had pairs of samples with compositions of pyrope with 75 % pyrope ($py_{75}mj_{25}$), and 75 % pyrope with 50 % pyrope ($py_{50}mj_{50}$); an experiment with a pure majorite sample was attempted but the majorite transformed to enstatite. The successful T-Cup experiments were undertaken in 7/3 and 7/2 cells respectively; the cell design for both experiments was the same and is illustrated in figure 2b. The majorite-containing starting samples were made from synthetic end-member pyrope (py_{100}) and majorite (mj_{100}) glasses which were mixed then repeatedly glassed in air at 1600 °C and ground under acetone until homogeneous. These glasses were then transformed into garnets at pressure and approximately 1400 °C in a 1000 tonne multi-anvil press at UCL; the recovered products were analysed by X-ray diffraction to confirm their crystal structure and phase purity. The recovered samples were ground for use as starting materials in the deformation experiments.

Each deformation experiment was conducted as follows. Prior to compression of the sample diffraction patterns were acquired from each sample in the cell for the measurement of a reference unit cell volume, V_0. The sample assembly was then compressed at room temperature to the required end load at which

point an X-radiograph and diffraction patterns from each sample were recorded. The cell was then heated to the desired temperature, and for the D-DIA experiment the active deformation was started; there was no annealing before deformation to remove compression damage. The elastic and macroscopic strains were observed throughout the experiment by the acquisition of a repeated sequence of alternate radiography and diffraction measurements. The exposure time of the images was of the order of tens of microseconds, and the time taken to collect each diffraction pattern was approximately 5 minutes. The temperature was increased when either: a few percent strain had been accumulated in the samples under the current conditions or, in the stress-relaxation experiments, the samples had stopped straining.

3. Data analysis

Diffraction patterns were analysed for phases present and unit cell parameter using plot85 and the axial and radial elastic strains calculated. Calculation of the elastic strains requires the thermal expansion of the samples; the value taken for the volumetric thermal expansion was that of pyrope ($19.9 \times 10^{-6}\,\mathrm{K}^{-1}$; Fei 1995) and was assumed to be independent of pressure, temperature and composition. The stresses can then be calculated, for an aggregate of randomly orientated cubic polycrystals in an axi-symmetric stress field (Nye 1985, page 143):

$$\sigma_a = c_{11}\varepsilon_a + 2c_{12}\varepsilon_r \tag{1a}$$

$$\sigma_r = c_{11}\varepsilon_r + c_{12}(\varepsilon_a + \varepsilon_r) \tag{1b}$$

where σ_a and σ_r are the stresses in the axial and radial directions respectively, ε_a and ε_r are the crystallographic strains in the same directions. The values c_{11} and c_{12} are the elastic constants (generically c_{ij}) for the samples, at the conditions of the measurement; no averaging of the elastic constants is needed because garnet is cubic.

The c_{ij} values used in this study are taken to change as a function of pressure, temperature and majorite content, according to the relationship:

$$c_{ij}^{P,T,X_{\mathrm{mj}}} = c_{ij}^{0} + P\frac{\partial c_{ij}}{\partial P} + T\frac{\partial c_{ij}}{\partial T} + X_{\mathrm{mj}}\frac{\partial c_{ij}}{\partial X_{\mathrm{mj}}} \tag{2}$$

where P is the pressure, T is the temperature, c_{ij}^{0} are the c_{ij} values of pure pyrope at room pressure and temperature. X_{mj} is the majorite content of the garnet, which as is defined as:

$$X_{\mathrm{mj}} = \frac{[\mathrm{mj}]}{[\mathrm{mj}] + [\mathrm{py}]} \tag{3}$$

and [mj] and [py] are the molar proportions of majorite and pyrope in the samples.

The c_{ij}^{0} values and their composition derivatives ($\partial c_{ij}/\partial X_{\mathrm{mj}}$) have been derived (using Lamé's relationships, e.g. Poirier 2000, pages 13-14) from a weighted fit to values of the bulk (K) and shear (μ) modulae for the pyrope–majorite solid solution taken from the literature (figure 1). The dependency of c_{ij} with majorite content ($\partial c_{ij}/\partial X_{\mathrm{mj}}$) and the value for pure pyrope (c_{ij}^{0}) can be interpolated from the

	Continuous composition derivatives		Discontinuous composition derivatives			
	All majorite contents		High majorite ($X_{\mathrm{mj}} > 0.67$)		Low majorite ($X_{\mathrm{mj}} \leqslant 0.67$)	
	Value at $X_{\mathrm{mj}} = 0$	$\partial/\partial X_{\mathrm{mj}}$	Value at $X_{\mathrm{mj}} = 0$	$\partial/\partial X_{\mathrm{mj}}$	Value at $X_{\mathrm{mj}} = 0$	$\partial/\partial X_{\mathrm{mj}}$
K	172.9 ± 0.3	-10.9 ± 0.7	168.9 ± 5.5	-6.7 ± 6.0	172.9 ± 0.3	-10.9 ± 0.7
μ	91.6 ± 0.2	-3.7 ± 0.3	81.4 ± 2.7	7.3 ± 2.9	91.7 ± 0.2	-4.7 ± 0.8

Table 1: Composition dependencies of $K_{X_{\mathrm{mj}}}$ and $\mu_{X_{\mathrm{mj}}}$ on majorite content, where $X_{\mathrm{mj}} = [\mathrm{mj}]/([\mathrm{mj}] + [\mathrm{py}])$. The numbers presented here are those that describe the fits in figures 1a and b. The units of the intercept values and slopes are GPa and GPa/X_{mj} respectively.

c_{ij}	$c_{ij,X_{\mathrm{mj}}=0}$ (GPa)	$\frac{\partial c_{ij}}{\partial P}$	$\frac{\partial c_{ij}}{\partial T}$ (GPa K^{-1})	$\frac{\partial c_{ij}}{\partial \%\mathrm{Mj}}$ (GPa $X_{\mathrm{mj}}{}^{-1}$)
c_{11}	295.0 ± 0.3	6.9 ± 0.1	-0.033 ± <0.001	-16.4 ± 0.9
c_{12}	111.8 ± 0.5	3.5 ± 0.1	-0.013 ± <0.001	-72.0 ± 1.2
c_{44}	91.6 ± 0.2	1.8 ± 0.1	-0.010 ± <0.001	-37.0 ± 0.3

Table 2: Table of the isotropic c_{ij} values used in this study to calculate the stresses in the garnet samples from the elastic strains. For details of the origin of the numbers see text; the data from which these data are derived are listed in the caption for figure 1.

published data by assuming either that the composition dependency is continuous (solid lines, figure 1) or that there is a discontinuity in the composition dependency (dashed lines, figure 1). A discontinuity in $\partial K/\partial X_{\mathrm{mj}}$ and $\partial \mu/\partial X_{\mathrm{mj}}$ is preferred by Sinogeikin et al. (1997) on the basis that a cubic-tetragonal transition occurs in pyrope–majorite garnets at ambient conditions and $X_{\mathrm{mj}} = 0.67$. However, they could not exclude the possibility that the modulae decrease continuously across the solid solution. Heinemann et al. (1997) concluded that the cubic-tetragonal transition in pyrope–majorite garnets, a likely source for any discontinuity in the composition derivative, does not occur at high pressures and temperatures in majorite rich garnets. Therefore, in the present study, the composition derivatives of the moduli are considered to be continuous across the entire solid solution, particularly since the composition of the present samples were less than $X_{\mathrm{mj}} = 0.5$. The weighted least-squares fits to the data giving the changes in K and μ as a function of majorite content in pyrope, both with and without a discontinuity, are presented in table 1; the data which were published without errors have been left out of the analysis, although they are included in figure 1.

Measurements of the pressure derivatives of K and μ ($\partial K/\partial P$ and $\partial \mu/\partial P$) as a function of majorite content are not as numerous as measurements of merely the modulae; the papers which include pressure dependency data are: Duffy and Anderson (1989), Rigden et al. (1994), Gwanmesia et al. (1998), Wang et al. (1998), Chen et al. (1999), Lui et al. (2000), Wang and Ji (2001), Sinogeikin and Bass (2002a), Gwanmesia et al. (2006). There is no definitive composition dependency to the pressure derivatives of c_{ij} demonstrated by these data and therefore the pressure derivatives are calculated as a weighted fit to the published $\partial K/\partial P$ and $\partial \mu/\partial P$ values assuming that there is no composition dependence. The temperature derivatives of the c_{ij} values ($\partial c_{ij}/\partial T$) are isotropic Hill averages of the single crystal data for the 'pyrope-rich garnet' in Anderson and Isaak (1995); they are also assumed to be independent of composition. All other higher order derivatives are assumed to be negligible. A summary of the c_{ij} values and their derivatives used in this study is presented in table 2.

The change in the length of the samples throughout the experiment was calculated, from the radiographs, by the cross-correlation method described previously by Li et al. (2003). From these length changes the sample strains can be calculated, the errors of which are estimated assuming that; (1) there is a 5 pixel error in the starting length of the sample, and (2) the error in length change between two adjacent images is 0.05 pixels. This radiographically measured strain ($\Delta l/l_0$) contains a recoverable elastic strain component, as well as a component due to unrecoverable plastic strain. During deformation at constant stress and temperature (in the D-DIA) the elastic strain is constant and the plastic strain-rate is equal to the observed bulk strain-rate. This is not the case for stress-relaxation experiments (in the T-Cup) where both the elastic and plastic strains vary simultaneously; consequentially the strain-rates measured by radiography are not necessarily equal to the true plastic strain-rates in the samples. Therefore, to calculate the instantaneous plastic strain-rates we first calculate the true instantaneous plastic-strains using the procedure of Durham et al. (2002), who define the plastic strain developed during some time interval as:

$$\varepsilon = \frac{R_{k,n} - R_{k,n+1}}{R_{k,n}} \tag{4a}$$

where R_k is the so called Kung ratio:

$$R_k = \frac{l_n}{l_0} / \frac{a_n}{a_0} \tag{4b}$$

The sample length is l, a is the axial unit-cell length measured by diffraction and the subscript n denotes the values at time n. The ratio R_k is the compliment of the bulk strain which would be observed if the sample was instantly relaxed to zero stress and room temperature at the time of the measurement.

In order to calculate R_k properly the values of a and l need to be coincident in time, which in the raw data they are not. Therefore, the axial crystallographic length (a in equation 4b) was calculated at the time of the radiography measurements by interpolation. The plastic strains and instantaneous strain-rates were then calculated from R_k for each sample. The ratios of the instantaneous strain-rates from the T-Cup and D-DIA experiments were then used to determine the effect of temperature and composition on the strength of the garnet solid-solution.

The experimental data in this study were not sufficiently constrained or abundant to determine independent flows law for pyrope-majorite garnets. However, with some manipulation, the ratio of the strain-rates of the pyrope and majoritic samples can be used to derive a flow law for majorite-containing garnets relative to the flow law for pure pyrope. This relative flow law can then be combined the with flow laws of previous studies on pure pyrope (Dobson et al. 2005, Li et al. 2006) to give a flow law for the entire pyrope–majorite solid solution, which is important for mantle garnet compositions. The flow law for majoritic garnet relative to that for pyrope is derived from the flow laws for the two separate phases as follows. We assume a generic flow-law for plastic deformation of:

$$\dot{\varepsilon} = A_0 \sigma^n \exp\left(\frac{-Q}{RT}\right) \tag{5}$$

where $\dot{\varepsilon}$ is the strain rate, A_0 is the pre-exponential factor, σ the differential stress, n the stress exponent, Q is the activation energy for creep, R the gas constant and T the absolute temperature; this is the flow-law generally applied to climb-assisted dislocation glide deformation. Rearranging this equation for Q and taking the difference between the two relationships for majoritic and pyrope garnets gives the difference between the activation energies of majoritic and pyrope garnet:

$$Q^{X_{\mathrm{mj}}} - Q^{\mathrm{py}} = -\frac{(\log \dot{\varepsilon}^{X_{\mathrm{mj}}} - \log A_0^{X_{\mathrm{mj}}} - n^{X_{\mathrm{mj}}} \log \sigma) - (\log \dot{\varepsilon}^{\mathrm{py}} - \log A_0^{\mathrm{py}} - n^{\mathrm{py}} \log \sigma)}{\frac{1}{\mathrm{R}T}} \tag{6}$$

where the superscripts 'X_{mj}' and 'py' denote the majorite- and pyrope-rich phases respectively. Under the experimental conditions the stresses in both the samples are the same and assuming that the stress dependency does not change as a function of majorite content (*i.e.* $n^{X_{\mathrm{mj}}} = n^{\mathrm{py}}$) the stress dependencies cancel. By also assuming that the A_0 values have no temperature dependency, which is true for a simple Arrhenius process, the equation above simplifies to:

$$\begin{aligned} Q^{X_{\mathrm{mj}}} - Q^{\mathrm{py}} &= -\left[\frac{\partial(\log \dot{\varepsilon}^{X_{\mathrm{mj}}} - \log \dot{\varepsilon}^{\mathrm{py}})}{\partial \frac{1}{\mathrm{R}T}}\right]_{\sigma} \\ &= -\left[\frac{\partial \log(\frac{\dot{\varepsilon}^{X_{\mathrm{mj}}}}{\dot{\varepsilon}^{\mathrm{py}}})}{\partial \frac{1}{\mathrm{R}T}}\right]_{\sigma} \end{aligned} \tag{7}$$

It is therefore possible to calculate the differences in activation energy and pre-exponential factors for high-temperature creep in pyrope and majoritic garnets.

The activation energy (Q) can be split into two parts: the activation enthalpy (E^*) and an activation volume (V^*):

$$Q = E^* + PV^* \tag{8}$$

where P is the pressure. If the activation volumes for pyrope and majoritic garnets are identical the activation energy (Q) in equation 7 is independent of pressure because the PV^*_{py} and $PV^*_{X_{\mathrm{mj}}}$ terms cancel. For the experiments conducted here, no correlation between the strain-rate ratios and the measured pressure was discernible in the experimental data. Therefore, it has been assumed that the volume of activation is constant across the solid solution ($V^*_{\mathrm{py}} = V^*_{X_{\mathrm{mj}}}$) and has no effect on the strain-rate ratio.

4. Results

The three successful synchrotron experiments undertaken in this study were analysed to find the ratio of the strain-rates for the two samples during the experiment and the results are presented in table 3 as a function of temperature. The data were analysed in slightly different manners for the D-DIA (Garn_33) and T-Cup experiments but the data from the two T-Cup experiments (Garn_35 and 36) were analysed in an identical manner.

D-DIA experiment — py_{100}–$py_{95}mj_5$ (Garn_33)

The first experiment was undertaken in the D-DIA with samples of py_{100} and $\mathrm{py}_{95}\mathrm{mj}_5$ with constant strain-rates. The pressure and differential stresses during this experiment were constant at each set

	Run #	Samples	T (°C)	P (GPa)	σ (GPa)	$\dot{\bar{\varepsilon}}_{X_{mj}}$ ($\times 10^{-6}s^{-1}$)	$\dot{\bar{\varepsilon}}_{py}$ ($\times 10^{-6}s^{-1}$)	Ratio ($\dot{\varepsilon}_{X_{mj}}/\dot{\varepsilon}_{py}$)
D-DIA	Garn_33	$py_{95}mj_5$	800	9.2 ± 0.2	1.4 ± 0.1	2.05 ± 0.05	2.38 ± 0.05	0.86 ± 0.03
		py_{100}	1000	8.7 ± 0.1	1.4 ± 0.1	4.99 ± 0.04	5.05 ± 0.03	0.98 ± 0.01
			1200	7.9 ± 0.1	1.4 ± 0.1	6.85 ± 0.06	6.13 ± 0.04	1.12 ± 0.01
T-Cup	Garn_35	$py_{75}mj_{25}$	500	9.5 ± 0.2	2.4 ± 0.1	3.2 ± 1.2	2.3 ± 0.8	1.38 ± 0.41
		py_{100}	600	11.4 ± 0.1	1.0 ± 0.1	4.7 ± 1.5	8.1 ± 2.6	0.58 ± 0.14
			775	13.3 ± 0.1	0.4 ± 0.1	11.7 ± 1.3	14.9 ± 1.5	0.78 ± 0.06
			850	13.6 ± 0.1	0.2 ± 0.1	4.4 ± 0.3	1.0 ± 0.2	4.65 ± 0.50
			900	12.5 ± 0.1	$< 0.1 \pm 0.1$	–	–	
	Garn_36	$py_{50}mj_{50}$	600	12.9 ± 0.2	2.5 ± 0.2	10.8 ± 2.6	11.5 ± 3.7	0.94 ± 0.22
		$py_{75}mj_{25}$	670	11.5 ± 0.2	0.5 ± 0.1	1.4 ± 0.3	8.9 ± 1.0	0.16 ± 0.02
			720	11.9 ± 0.2	0.2 ± 0.1	3.4 ± 0.4	7.5 ± 0.7	0.45 ± 0.04
			770	10.5 ± 0.1	$< 0.1 \pm 0.1$	3.2 ± 0.3	6.2 ± 0.4	0.51 ± 0.03
			920	7.6 ± 0.1	$< 0.1 \pm 0.1$	2.8 ± 0.2	0.8 ± 0.2	3.95 ± 0.60

Table 3: Strain rates and experimental conditions for the pyrope-majorite relative strength experiments. The strain-rates presented here for the Garn_35 and 36 are the arithmetic averages of the instantaneous strain-rates and as such are only included to give an indication of the actual strain-rates in the experiment; strain-rate ratios for the stress-relaxation experiments are the average of the instantaneous strain-rate ratio at those conditions. The data in this table have been plotted in figure 7.

of conditions (table 3) and therefore it is possible to calculate the plastic-strains directly from the radiography images, rather than *via* the Kung ratio (equations 4a and 4b). Measured strains are plotted in figure 3.

The sample strain-rates ($\dot{\varepsilon}_{X_{mj}}/\dot{\varepsilon}_{py}$) changes systematically with temperature (table 3). The first data point after heating (grey points in figure 3) were excluded from the strain-rate calculations in order to avoid including the transient effects that result from heating. The strain-rate ratio decreases with increasing temperature; at 800°C the $py_{95}mj_5$ garnet is weaker than pyrope but at 1200°C the reverse is true.

T-Cup experiments — py_{100}–$py_{75}mj_{25}$ (Garn_35) and $py_{75}mj_{25}$–$py_{50}mj_{50}$ (Garn_36)

Two stress-relaxation experiments were performed in the T-Cup, with higher majorite contents in the garnets and at higher pressure than the experiment in the D-DIA. To calculate the plastic component of the strains from these stress-relaxation experiments it was necessary to use the Kung ratio (equations 4a and 4b); the resulting plastic strains are plotted in figures 4a (Garn_35) and 5 (Garn_36). The plastic strains calculated in this way differ from the strains calculated directly from the radiography images by between 1 and 2 % with most of this difference occuring during initial heating of the samples.

The most significant feature of the plastic strain in Garn_35 (samples: py_{100} and $py_{75}mj_{25}$) is that there is a significant increase in the strain accommodated by both samples upon increasing the temperature from 600 to 775 °C. This temperature range is consistent with the weakening observed in garnets by Weidner et al. (2001). As with Garn_33, above 600 °C, there is a weakening of majorite-rich garnets relative to pyrope with increasing temperature.

The increase in strain with time during the experiment is more monotonic in Garn_36 than Garn_35 but similar features can be observed in the data. At 600°C the strain-rates are approximately the same,

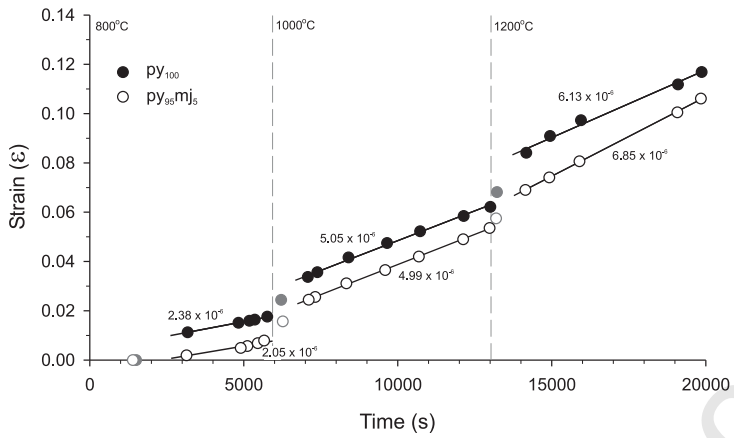

Figure 3: Strain as a function of time during experiment Garn_33. The filled symbols are for the py_{100} sample and the open symbols are the $py_{95}mj_5$ sample; the grey symbols indicate those data points not used in the calculation of the strain-rates; the first black point at each temperature was used as the l_0 in the strain calculation.

between 670 and 770°C the $py_{50}mj_{50}$ sample has a slower strain-rate than the more pyrope rich sample and at 900°C the $py_{75}mj_{25}$ sample almost stops straining, whist the $py_{50}mj_{50}$ continues to deform. Above 770°C in Garn_36 the differential stresses became too small to measure, but the samples continued to strain in a manner consistent with the rest of the experimental results. Moreover, at room temperature the more majorite-rich sample supported a higher differential stress (6.5 ± 0.4 GPa in the $py_{50}mj_{50}$ sample as opposed to 1.7 ± 0.9 GPa in the $py_{75}mj_{25}$ sample). This is consistent with the observations of Kavner et al. (2000), who observed that majoritic garnets support a very large differential stress at room temperature.

The confining pressures throughout Garn_35 are high enough for the $py_{75}mj_{25}$ sample to be stable but in Garn_36 the pressures drop below the ≈12.8 GPa pressure required for the $py_{75}mj_{25}$ garnet to be in its stability field. At the temperatures of these experiments the kinetics of the decomposition reaction proved to be too slow for enstatite to form, indeed no enstatite peaks were observed in any of the diffraction patterns. We note here that a further experiment, Garn_37, was performed with pure majorite as one of the samples; this sample was observed to transform to pyroxene at ≈11.4 GPa and 550°C. For all the experiments, the difference between the pressures measured from the two samples were for the most part within two standard deviations of each other (figure 4b shows the pressures measured during Garn_35); the same is true for the differential stresses at high temperature (figure 4c – differential stresses from Garn_35). The mean pressures and differential stresses for each temperature in all the experiments are listed in table 3.

Recovered samples

Figure 6 presents two secondary electron images of the samples recovered from experiment Garn_36; these images are typical of the recovered samples from all the experiments reported here. In these images it can be observed that the grains are between 1 and 5 μm in size, with a mean of approximately 2 μm.

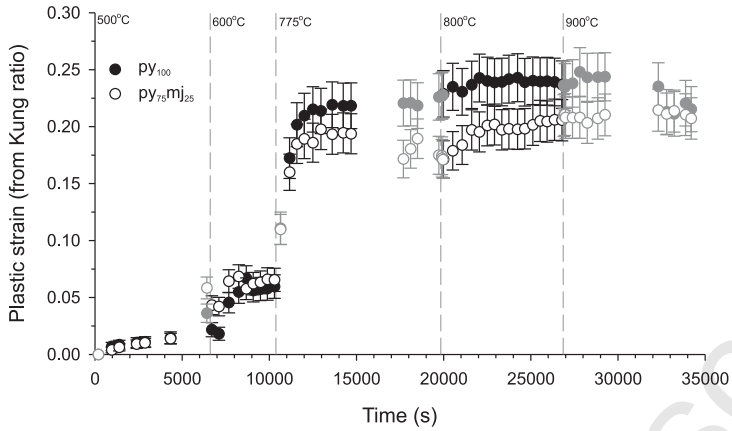

(a) Plastic strain (from R_k)

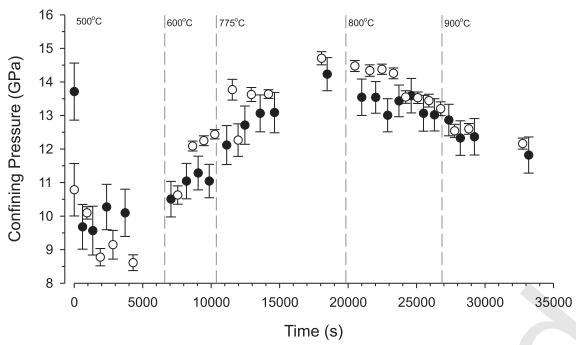

(b) Confining pressure

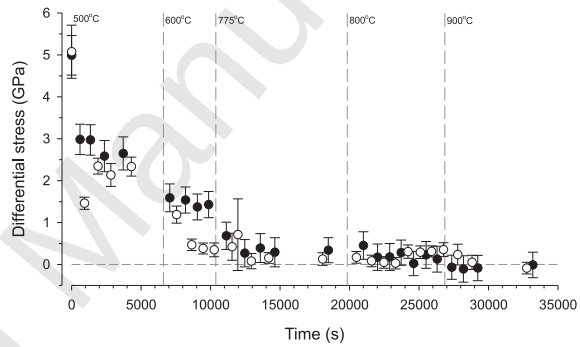

(c) Differential stress

Figure 4: Strain and stresses during experiment Garn_35. The filled symbols are for the py_{100} sample and the open symbols are the $py_{75}mj_{25}$ sample; the vertical dashed lines indicate the time at which the temperature was increased to the values adjacent to the lines. The grey symbols in part (a) indicate data points not used in calculating the ratios of the strain rates.

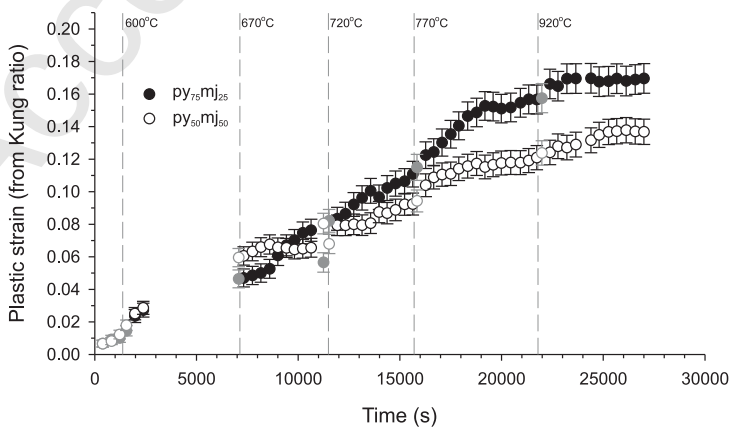

Figure 5: Strain and stresses during experiment Garn_36. The filled symbols are for the $py_{75}mj_{25}$ sample and the open symbols are the $py_{50}mj_{50}$ sample; the vertical dashed lines indicate the time at which the temperature was increased to the values adjacent to the lines. The grey symbols indicate data points not used in calculating the ratios of the strain rates.

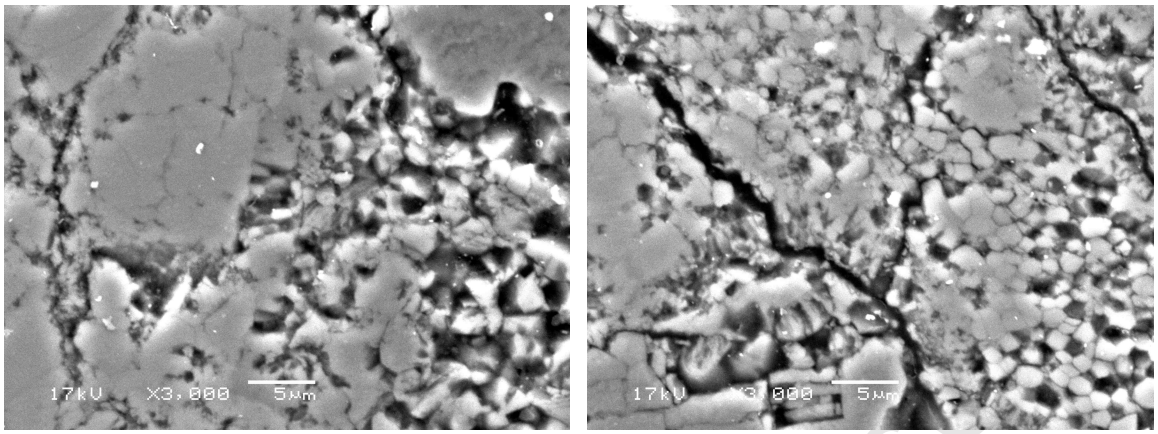

Figure 6: SEM micrographs of the recovered samples from experiment Garn_36; the left-hand image is of the $py_{75}mj_{25}$ sample and the right-hand image of the $py_{50}mj_{50}$ sample.

Experiment	Garn_33	Garn_35	Garn_36	35 & 36 combined
Sample 1	py_{100}	py_{100}	$py_{75}mj_{25}$	py_{100}
Sample 2	$py_{95}mj_{5}$	$py_{75}mj_{25}$	$py_{50}mj_{50}$	$py_{50}mj_{50}$
$Q^{X_{mj}} - Q^{py}$	3.9 ± 0.4	101.0 ± 7.4	57.1 ± 4.3	158.1 ± 8.5
$\log A_0^{X_{mj}} - \log A_0^{py}$	0.37 ± 0.03	11.48 ± 0.83	6.31 ± 0.49	17.79 ± 0.96

Table 4: Activation energy differences and A_0 values for the pyrope–majorite experiments. These fits are the lines that are plotted in figure 7.

the similarity of the grain-sizes between the two samples means that it is unlikely that the difference in strength between samples is due to crystal superplasticity.

Strain-rate ratios

The ratio of the instantaneous strain-rates of the two pairs of samples in each experiment were calculated (table 3) excluding the data highlighted in grey in figures 3, 4 and 5. These data have been excluded because either they are immediately after heating of the samples and so will incorporate transient effects or the sample is not straining significantly under the conditions. The resulting ratios are plotted in figure 7. The most obvious feature in this graph is the change in behaviour above and below ≈ 650°C ($1/RT \approx 1.30 \times 10^{-4}$ mol J^{-1}). Below 650 °C the strain-rate ratio measurements show no strong temperature dependency and the mean value (0.97 ± 0.16) is within error of unity, whilst above 650°C there is a clear temperature dependency. In Garn_35 and 36, above 800°C the more majoritic samples are weaker (i.e. straining faster) than the pyrope samples, whereas between 650 and 770°C the pyrope-rich samples are weaker. The D-DIA experiment (Garn_33) follows a similar pattern however the majoritic sample is weaker above 1050°C and stronger below this temperature.

The temperature at which the strain-rate ratios change from being temperature independent to temperature dependant is about 650°C. This is within the temperature range for the change in deformation mechanism from dislocation glide to climb-assisted dislocation glide (after Dobson et al. 2005), and approximately the temperature above which cation diffusion in metamorphic garnets becomes significant

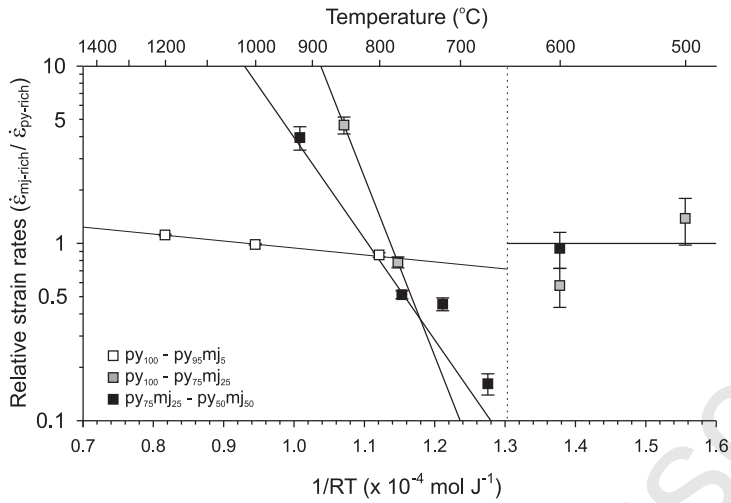

Figure 7: Ratio of the strain-rates in the pyrope and py-mj samples against 1/RT for experiments in this study, where T is the absolute temperature. The vertical dotted line is the approximate temperature at which the deformation mechanism changes from dislocation glide to climb and the errors of the offline experiments have been omitted because of their size. The data plotted here is presented in table 3 and the weighted fits to the data are presented in table 4.

(Yardley 1977). Moreover, around this temperature, depending on the strain rate, there is a change in the microstructure of both naturally and experimentally deformed garnets (Voegelé et al. 1998a,b).

Above 650°C the strain-rate ratios become sensitive to temperature and at these temperatures climb-assisted dislocation glide is the dominant deformation-mechanism (Li et al. 2006). Between 650 and 800°C majoritic garnets are stronger than pyrope; however, this does not mean that there is an increase in the absolute strength of majoritic garnets but only that the majorite phase has weakened less than the pyrope as the deformation mechanism changes from dislocation glide to climb-assisted glide, indeed there is a 10-fold weakening in Garn_35 between 600 and 750°C. The strain-rate ratios of the py_{100}–$py_{95}mj_5$ experiment show a smaller temperature dependence than the other experiments which have a 25 %-majorite difference between the samples and the $py_{75}mj_{25}$–$py_{50}mj_{50}$ has a lower dependency on temperature than the py_{100}–$py_{75}mj_{25}$ experiment.

Flow-law for majorite containing garnets

From the strain-rate ratios (figure 7, table 3) the activation energy (Q) of majoritic garnets relative to that of pyrope has been calculated, using equation 7. These activation energy differences, calculated from a weighted fit to each set of experimental data above 650°C, are presented in table 4; the differences between the logarithms of pre-exponential factors ($\log A_0$) are also included in the table. In the final column in table 4 the values from experiments Garn_35 and 36 are summed to give the differences in activation energy and logarithms of the pre-exponential factors between pyrope and $py_{50}mj_{50}$.

From these activation energy differences the change in activation energy as a function of majorite content across the entire pyrope-majorite solid solution can be derived assuming that the cubic–tetragonal transition does not have a significant effect on rheology or that it does not occur at elevated pressures

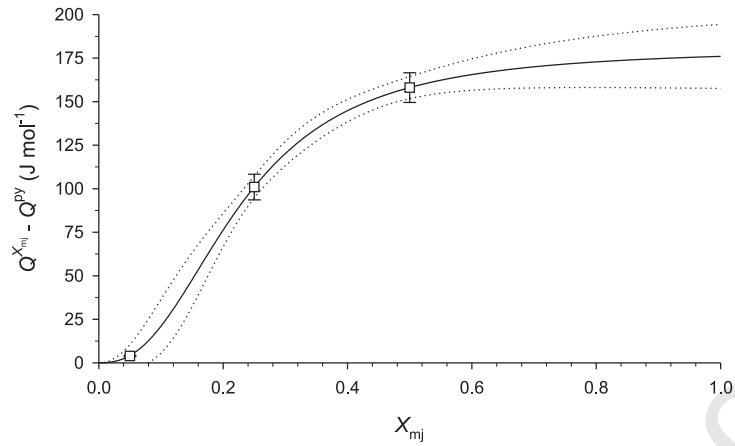

Figure 8: Activation energy difference for the pyrope–majorite solid-solution as a function of majorite content in the high temperature regime (T> 650°C); the solid line is the fit to the data defined by equation 9c and the dashed lines are one the standard error boundaries of the fit. The errors on the data points are the weighted fits presented in table 4.

and temperatures (after Heinemann et al. 1997). The activation energy differences between pyrope and majoritic garnets have been plotted as a function of X_{mj} in figure 8.

The functional form of the activation energy difference between pyrope and majoritic garnets is not known and no previous work has been found in which the expected functional form has been derived. However, there are various constraints on the function which the relationship must have beyond the values of the data. The function $Q^{X_{\mathrm{mj}}} - Q^{\mathrm{py}}$ must be zero at $X_{\mathrm{mj}} = 0$. For both 'low' and 'high' majorite contents there is expected to be relatively little change in the activation energy for creep as a function of X_{mj} because the occupancy of the octahedral site will be dominated by Al^{3+} or Si^{4+} and Mg^{2+} respectively. Most of the change in activation energy will therefore be at at 'intermediate' compositions, but what constitutes 'low', 'intermediate' and 'high' compositions is not known *a priori*. These constraints define the activation energy to be a sigmoidal function of majorite content. The best fitting function (solid line in figure 8) was found to be an asymmetric sigmoid and has the form:

$$Q^{X_{\mathrm{mj}}} - Q^{\mathrm{py}} = a\left(\frac{b \cdot {X_{\mathrm{mj}}}^{c}}{1 + b \cdot {X_{\mathrm{mj}}}^{c}}\right)$$

where a, b and c are constants.

This relationship has the same form as the Hill equation (Hill 1910, who used it to describe oxygen ligand bonding to haemoglobin). Significantly however, this function passes through zero at no majorite content and has by far the lowest least squares misfit of all the functions tried. Moreover, the function does not asymptote with increasing majorite content. The sparsity of the data and the errors on the activation energy differences do not preclude the possibility that the actual functional form of the relationship is different from that used here. A similar analysis has been performed for the value of the pre-exponential factor difference assuming that both pyrope and majorite have the same stress dependencies and, again, the Hill equation has the smallest least squares residual of all the functions tried.

Combined, these relationships define the flow law for majoritic garnets relative to that of pyrope to

be:

$$\dot{\varepsilon}_{X_{\mathrm{mj}}} = \begin{cases} \dot{\varepsilon}_{\mathrm{py}} & \text{when } T < 650^\circ\mathrm{C}, \\ A_0^{X_{\mathrm{mj}}} \sigma^n \exp\left(\frac{-Q^{X_{\mathrm{mj}}}}{\mathrm{R}T}\right) & \text{when } T \geqslant 650^\circ\mathrm{C}. \end{cases} \tag{9a}$$

where

$$\log A_0^{X_{\mathrm{mj}}} = \log A_0^{\mathrm{py}} + 19.9(13)\left(\frac{51.8(489)\cdot {X_{\mathrm{mj}}}^{2.6(6)}}{1 + 51.8(489)\cdot {X_{\mathrm{mj}}}^{2.6(6)}}\right) \tag{9b}$$

$$Q^{X_{\mathrm{mj}}} = Q^{\mathrm{py}} + 180.5(119)\left(\frac{39.1(319)\cdot {X_{\mathrm{mj}}}^{2.5(5)}}{1 + 39.1(319)\cdot {X_{\mathrm{mj}}}^{2.5(5)}}\right) \tag{9c}$$

For reference the flow law for pyrope at less than 650°C has been measured by Dobson et al. (2005) and at greater than 650 °C by Li et al. (2006) who measured $Q^{\mathrm{py}} = 270 \pm 40\,\mathrm{kJ\,mol^{-1}}$ and $A_0^{\mathrm{py}} = 3.5^{+4.8}_{-2.0} \times 10^6 \mathrm{s}^{-1}$. Therefore the activation energy for climb-assisted dislocation glide in end-member majorite according to this study is $446 \pm 44\,\mathrm{kJ\,mol^{-1}}$.

5. Discussion

Mineral physics

The relationship between the strength of pyrope and majoritic garnets is more complex than initially expected. A change in relative strength with composition was expected but the temperature effect was not; in hindsight perhaps it should have been. Such temperature dependant behaviour has not been predicted previously but we are confident that the temperature effects observed here are robust and not an artefact derived from pressure effects. If all the experiments saw a reduction in sample pressure with increasing temperature we would be unable to distinguish between a pressure and temperature dependant rheology. However we saw the same temperature-dependent trend of strength in all experiments despite the pressure increasing slightly (Garn_35), dropping slightly (Garn_33) and dropping significantly (Garn_36). This suggests that the pressure effect is small, supporting our neglect of the PV^* term, in equation 8.

The change in strength between pyrope and majoritic garnets is clear to see in figure 7. At low temperatures (< 650°C) majoritic garnets have the same flow law as pyrope while at higher temperatures the flow law of majoritic garnets is significantly dependent on the majorite content of the garnet and the temperature (equation 9). The flow law derived here is consistent with a change in deformation mechanism in both pyrope and majoritic garnets at about 650°C. This is in agreement with the studies of Yardley (1977), Voegelé et al. (1998a,b), Dobson et al. (2005) among others, all of whom make arguments related to a change in deformation mechanism at about this temperature.

The relative flow-law presented here, in equation 9, is valid assuming that the stress dependences (n) of pyrope and majoritic garnets are the same. In the calculation for the flow-law if they are the same they cancel but if not the pre-exponential factor as formulated here has a stress dependant term in it. It cannot, however, be discerned from this data set if there is a change in n with majorite composition.

We suggest the observed composition dependence of majorite rheology might be explained as follows: strain-rate, under a given differential stress, in the dislocation-climb regime is controlled by diffusion of the chemical species. By adding Si onto the nominal 3+ site in garnet it becomes easier to create cation vacancies by local charge-balancing with Si^{4+}, increasing the vacancy concentration. This, in turn, increases the the pre-exponential factor in the strain-rate Arrhenius equation (equation 9b). However, adding silicon to the 3+ site also increases the migration enthalpy, resulting in an increase in the magnitude of the exponential term; hence the steeper gradients in figure 7 as a function of increasing majorite content. These two effects combine such that at temperatures above approximately 800°C highly majoritic garnets are weaker than pyrope.

Rheology of the mantle

In normal mantle, i.e. away from subduction zones, the highest garnet component of the mineralogy is in the transition-zone, at depths of about 520 km (Ringwood 1991), where the temperatures are between 1600 and 1700°C. At these conditions, majoritic garnets in the transition zone will be much weaker than pure pyrope would be at the same conditions. This, combined with the increased strength of the high pressure polymorphs of olivine (e.g. Weidner et al. 2001) relative to that of olivine, shows that majoritic garnets will be the weak phase in the transition zone; a conclusion which is contrary to the predictions of Karato et al. (1995) and Kavner et al. (2000).

Thermal models show that at transition zone depths the top-most layer of the subducting slab is at temperatures in excess of 800°C. Therefore any majoritic garnets in the MORB layer of the subducting slab will be weaker than if they were pure pyrope. Relative to the core of the slab, the MORB layer will be weaker because of the elevated temperatures and the weakening caused by the majorite component of the garnet. However, the weakening effect of majorite is unlikely to be sufficient to make the MORB layer weaker than the surrounding, non-subducting mantle because of the significant difference in temperature between the normal mantle ($T \approx 1600-1700$°C) and the top of the slab. Therefore, it is unlikely that this study invalidates previously published models of MORB layer delamination at the 660 km discontinuity (e.g. van Keken et al. 1996) but the relative viscosity of the garnet layer and the core of the subducting slab will be significantly reduced or even reversed and the models will need to be reassessed.

6. Summary and Conclusions

In this study we have measured the relative strength of garnets in the pyrope–majorite solid solution and shown that the strength of majorite relative to that of pyrope changes as a function of temperature and composition. A flow law for majorite has been enumerated (equation 9) and we conclude that the the activation energy for climb-assisted dislocation glide in end-member majorite is $446 \pm 44\,\mathrm{kJ\,mol^{-1}}$. At temperatures below 650 °C both pure pyrope and majoritic garnets have the same strength whilst above 650 °C we find that majoritic garnets are initially stronger than pure pyrope but weaken with increasing temperature and majorite content.

Furthermore, it has been shown here that using relative strength experiments the flow law for an entire solid solution can be determined from just a few experiments. Also in these experiments a flow law for iron-free majorite garnet has been determined without the need to perform experiments on pure majorite. This is therefore a potentially useful method to determine the flow laws of high pressure phases from the lower-pressure end of the solid solutions of which they are part.

Acknowledgements

We acknowledge funding from the following sources: EU, Marie Curie Fellowships contract HPMT-CT-2001-00231 (SAH), NERC (SAH, DPD), The Royal Society (DPD) and NSF grant EAR0809397 (LL). This research has been supported by a Marie Curie Fellowship of the European Community programme "Improving Human Research Potential and the Socio-economic Knowledge Base" under contract number HPMT-CT-2001-00231. Use of the National Synchrotron Light Source, Brookhaven National Laboratory, was supported by the U.S. Department of Energy, Office of Science, Office of Basic Energy Sciences, under Contract No. DE-AC02-98CH10886. We acknowledge two anonymous referees for their helpful comments which significantly improved the manuscript.

References

Anderson, D. L., Isaak, D. G., 1995. Elastic constants of mantle minerals at high temperature. In: Ahrens, T. J. (Ed.), Mineral Physics and Crystallography: A Handbook of Physical Constants. American Geophysics Union, pp. 64 – 97.

Armbruster, T., Geiger, C. A., Lager, G. A., 1992. Single-crystal X-ray structure study of synthetic pyrope almandine garnets at 100 and 293 K. American Mineralogist 77, 512 – 521.

Bass, J. D., Kanzaki, M., 1990. Elasticity of a majorite–pyrope solid solution. Geophysical Research Letters 17 (11), 1989 – 1992.

Chen, G., Cooke, J. A., Gwanmesia, G. D., Liebermann, R. C., 1999. Elastic wave velocities of $Mg_3Al_2Si_3O_{12}$-pyrope garnet to 10 GPa. American Mineralogist 84, 348 – 388.

Cohen, M. L., 1991. Predicting new solids and their properties. Philosophical Transactions of the Royal Society of London. Series A, Mathematical and Physical Sciences 334, 501 – 513.

Conrad, P. G., Zha, C.-S., Mao, H.-k., Hemley, R. J., 1999. The high-pressure, single-crystal elasticity of pyrope, grossular, and andradite. American Mineralogist 84, 374 – 383.

Dobson, D. P., Mecklenburgh, J., Alfe, D., Wood, I. G., Daymond, M. R., 2005. A new belt-type appratus for neutron-based rheological measurements at Gigapascal pressures. High Pressure Research 25 (2), 107 – 118.

Duffy, T. S., Anderson, D. L., 1989. Seismic velocities in mantle minerals and the mineralogy of the upper mantle. Journal of Geophysical Research 94 (B2), 1895 – 1912.

Durham, B., Weidner, D. J., Karato, S., Wang, Y., 2002. New developments in deformation experiments at high pressure. In: Karato, S., Wenk, H.-R. (Eds.), Plastic deformation of minerals and rocks. Vol. 51 of Reviews in mineralogy and geochemistry. Mineralogical Society of America, pp. 21 – 49.

Fei, Y., 1995. Thermal expansion. In: Ahrens, T. J. (Ed.), Mineral Physics and Crystallography: A Handbook of Physical Constants. American Geophysics Union, pp. 29 – 44.

Gilman, J. J., 2003. Electronic Basis of the Strength of Materials. Cambridge University Press, Cambridge, UK.

Gwanmesia, G. D., Chen, G., Liebermann, R. C., 1998. Sound velocities in $MgSiO_3$-garnet to 8 GPa. Geophysical Research Letters 25 (24), 4553 – 4556.

Gwanmesia, G. D., Lui, J., Chen, G., Kesson, S., Rigden, S. M., Liebermann, R. C., 2000. Elasticity of the pyrope ($Mg_3Al_2Si_3O_{12}$) – majorite ($MgSiO_3$) garnets solid solution. Physics and Chemistry of Minerals 27, 445 – 452.

Gwanmesia, G. D., Zhang, J., Darling, K., Kung, J., Li, B., Wang, L., Neuville, D., Liebermann, R. C., 2006. Elasticity of polycrystalline pyrope ($Mg_3Al_2Si_3O_{12}$) to 9 GPa and 1000 C. Physics of The Earth and Planetary Interiors 155, 179 – 190.

Heinemann, S., Sharp, T. G., Seifert, F., Rubie, D. C., 1997. The cubic-tetragonal phase transition in the system majorite ($Mg_4Si_4O_{12}$) – pyrope ($Mg_3Al_2Si_3O_{12}$), and garnet symmetry in the Earth's transition zone. Physics and Chemistry of Minerals 24 (3), 206 – 221.

Hill, A. V., 1910. The possible effects of aggregation of the molecules of haemoglobin on its dissociation curve. Journal of Physiology 40, 4 – 7.

Hunt, S. A., Weidner, D. J., Li, L., Wang, L., Walte, N., Brodholt, J. P., Dobson, D. P., 2009. Weakening of $CaIrO_3$ during the perovskite-post perovskite transformation. Nature Geoscience, 10.1038/NGEO663.

Karato, S., Wang, Z., Liu, B., Fujino, K., 1995. Plastic deformation of garnets: systematics and implications for the rheology of the mantle transition zone. Earth and Planetary Science Letters 130 (1), 13 – 30.

Kavner, A., Sinogeikin, S. V., Jeanloz, R., Bass, J., 2000. Equation of state and strength of natural majorite. Journal of Geophysical Research 105 (3), 5963.

Leger, J. M., Redon, A. M., Chateau, C., 1990. Compressions of synthetic pyrope, spessartine and uvaorite garnets up to 25 GPa. Physics and Chemistry of Minerals 17, 161 – 167.

Leitner, B. J., Weidner, D. J., Liebermann, R. C., 1980. Elasticity of single crystal pyrope and implications for garnet solid solution series. Physics of The Earth and Planetary Interiors 22, 111 – 121.

Li, L., Long, H., Raterron, P., Weidner, D. J., 2006. Plastic flow of pyrope at mantle pressure and temperature. American Mineralogist 91, 517 – 525.

Li, L., Raterron, P., Weidner, D. J., Chen, J., 2003. Olivine flow mechansims at 8 GPa. Physics of The Earth and Planetary Interiors 138, 113 – 129.

Lui, J., Chen, G., Gwanmesia, G. D., Liebermann, R. C., 2000. Elastic wave velocities of pyrope–majorite garnets ($Py_{62}Mj_{38}$ and $Py_{50}Mj_{50}$) to 9 GPa. Physics of The Earth and Planetary Interiors 120, 153 – 163.

Nye, J. F., 1985. Physical Properties of Crystals: their Representation by Tensors and Matrices, 2nd Edition. Oxford University Press, Oxford.

O'Neill, B., Bass, J. D., Rossman, G. R., Geiger, C. A., Langer, K., 1991. Elastic properties of pyrope. Physics and Chemistry of Minerals 17, 617 – 621.

Pacalo, R. E. G., Weidner, D. J., 1997. Elasticity of majorite, $MgSiO_3$, tetragonal garnet. Physics of The Earth and Planetary Interiors 99, 145 – 154.

Poirier, J. P., 2000. Introduction to the Physics of the Earth's Interior. Cambridge Universtiy Press, Cambridge.

Rigden, S. M., Gwanmesia, G. D., Liebermann, R. C., 1994. Elastic wave velocities of a pyrope-majorite garnet to 3 GPa. Physics of The Earth and Planetary Interiors 86, 35 – 44.

Ringwood, A. E., 1991. Phase transformations and their bearing on the constitution and dynamics of the mantle. Geochimica et Cosmochimica Acta 55, 2083 – 2110.

Sato, Y., Akaogi, M., Akimoto, S., 1978. Hydrostatic compression of the synthetic garnets pyrope and almandine. Journal of Geophysical Research 83, 335 – 338.

Sinogeikin, S. V., Bass, J. D., 2002a. Elasticity of majorite and a majorite-pyrope solid solution to high pressure: Implications for the transition zone. Geophysical Research Letters 29 (2), 1017 – 1021.

Sinogeikin, S. V., Bass, J. D., 2002b. Elasticity of pyrope and majorite-pyrope solid solutions to high temperatures. Earth and Planetary Science Letters 203, 549 – 555.

Sinogeikin, S. V., Bass, J. D., O'Neill, B., Gasparik, T., 1997. Elasticity of tetragonal end-member majorite and solid solutions in the system $Mg_4Si_4O_{12}$–$Mg_3Al_2Si_3O_{12}$. Physics and Chemistry of Minerals 24, 115 – 121.

Sumino, Y., Anderson, D. L., 1984. Elastic Constants of Minerals. In: Carmichael, R. S. (Ed.), Handbook of Pyhsical Properties of Rocks. Vol. 3. CRC Press, Boca Raton, Florida, pp. 39 – 137.

van Keken, P. E., Karato, S., Yuen, D. A., 1996. Rheological control of oceanic crust separation in the transition zone. Geophysical Research Letters 23 (14), 1821 – 1824.

Vaughan, M., Weidner, D. J., Wang, Y., Chen, J. H., Koleda, C. C., Getting, I. C., 1998. T-cup: A new high-pressure apparatus for X-ray studies. Review of High Pressure Science and Technology 7, 1520 – 1522.

Voegelé, V., Ando, J. I., Cordier, P., Liebermann, R. C., 1998a. Plastic deformation of silicate garnets I. high-pressure experiments. Physics of The Earth and Planetary Interiors 108, 305.

Voegelé, V., Cordier, P., Sutter, V., Sharp, T. G., Lardeaux, J. M., Marques, F. O., 1998b. Plastic deformation of silicate garnets II. deformation microstructures in natural samples. Physics of The Earth and Planetary Interiors 108, 319.

Wang, Y., Durham, B., Getting, I. C., Weidner, D. J., 2003. The deformation-DIA: A new apparatus for high temperature triaxial deformation to pressures up to 15 GPa. Review of Scientific Instruments 74 (6), 3002 – 3011.

Wang, Y., Weidner, D. J., Zhang, J., Gwanmesia, G., Liebermann, R. C., 1998. Thermal equation of state of garnets along the pyrope-majorite join. Physics of The Earth and Planetary Interiors 105 (1-2), 59.

Wang, Z., Ji, S., 2001. Elasticity of polycrystalline silicate garnets to pressure up to 3.0 GPa. American Mineralogist 86, 1209 – 1218.

Wang, Z., Shaocheng, J., 2000. Diffusion creep in fine-grained garnetite: implications for the flow strength of subducting slabs. Geophysical Research Letters 27, 2333.

Weidner, D. J., Chen, J., Xu, Y., Wu, Y., Vaughan, M. T., Li, L., 2001. Subduction zone rheology. Physics of The Earth and Planetary Interiors 127, 67 – 81.

Weidner, D. J., Vaughan, M. T., Wang, Y., Leinenweber, K., Liu, X., Yeganeh-Haeri, A., Pacalo, R. E., Zhao, Y., 1992. Large volume high pressure research using the wiggler port at NSLS. High Pressure Research 8 (5), 617 – 623.

Yardley, B. W. D., 1977. An emperical study of diffusion in garnet. American Mineralogist 62, 793 – 800.

Yeganeh-Haeri, A., Weidner, D. J., Ito, E., 1990. Elastic properties of the pyrope-majorite solid solution series. Geophysical Research Letters 17 (12), 2453 – 2456.

Zhang, L. H., Ahsbahs, A., Geiger, C. A., 1999. Single-srystal hydrostatic compression of synthetic pyrope, almandine, spessartine, grossular and andradite garnets at high pressures. Physics and Chemistry of Minerals 27, 52 – 58.

Relative strength of the pyrope–majorite solid solution and the flow-law of majorite containing garnets.

Simon A. Hunt*[,a,b], David P. Dobson[a], Li Li[c], Donald J. Weidner[c], John P. Brodholt[a]

[a] *Department of Earth Sciences, University College London, Gower Street, London. WC1E 6BT, UK*
[b] *Department of Chemistry, University College London, 20 Gordon Street, London. WC1H 0AJ, UK*
[c] *SUNY Stony Brook, Inst. Mineral. Phys., Dept. Geosci., Stony Brook, NY 11790 USA*

Abstract

Even though the garnet phase is the second most abundant phase in the upper-mantle and transition-zone, no previous studies have directly measured the effect of majorite content on the strength of garnet under mantle conditions. Here we report the results of constant strain-rate and stress-relaxation experiments on garnets in the pyrope–majorite solid solution which constrain the strength of majoritic containing garnets relative to pyrope as a function of majorite content and temperature. We find that at temperatures below 650 °C both pure pyrope and majoritic garnets have the same strength. Conversely, above 650 °C we find that majoritic garnets are initially stronger than pure pyrope but weaken with increasing temperature and majorite content and with significant majorite contents are weaker than pyrope above approximately 800 °C. We develop a flow law for the entire pyrope–majorite solid solution as a function of temperature and majorite content.

Key words: garnets, transition-zone, majorite rheology, flow-law, high-pressure, high-temperature

1. Introduction

This section has changed little in revision; references to experiments at the Bayerisches Geoinstitut have been removed.

The garnet phase is the second most abundant mineral component of the upper mantle and transition zone, after olivine and its high pressure polymorphs. In undifferentiated pyrolite mantle, the modal amount of garnet is about 15 % at depths of 100–300 km increasing to around 40 % between 500 and 600 km. In subducting slabs the percentage garnet in the MORB component of the slab can be as high as 90 % between depths of 450 and 550 km (Ringwood 1991). There is potential, therefore, for the garnet phase to have a significant influence on mantle dynamics. However, despite this there have been, to date, relatively few studies measuring the rheology of even pure pyrope, let alone other garnet compositions relevant to the mantle. Studies that have been undertaken measuring the flow of pyrope include Wang and Shaocheng (2000), Dobson et al. (2005) and Li et al. (2006).

The increasing amount of garnet with depth in the subducting slab and mantle is the result of the increased solubility of pyroxene (generically $AB(Si_2O_6)$, where A and B are the two cations) in garnet as

*Corresponding author: s.hunt@ucl.ac.uk

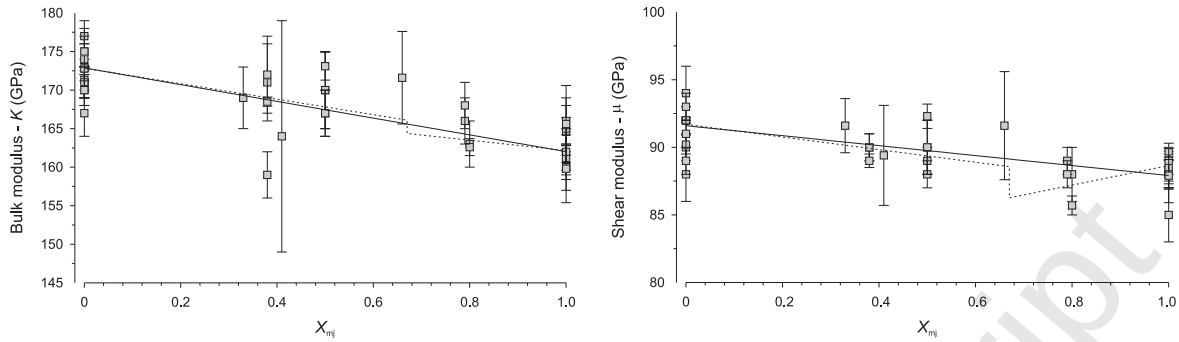

(a) Bulk modulus – K **(b)** Shear modulus – μ

Figure 1: Plot of K and μ values reported in the literature for the pyrope–majorite solid solution (updated after Sinogeikin et al. 1997), where $X_{\mathrm{mj}} = [\mathrm{mj}]/([\mathrm{mj}] + [\mathrm{py}])$. The solid lines are the weighted fit to all the data for which there are published errors and the dotted lines are the separate weighted fits to the data with majorite contents above and below 67 %, after the preferred fit of Sinogeikin et al. (1997). The coefficients for the solid and both parts of the dashed lines are presented in table 1. The data are taken from: Sato et al. (1978), Leitner et al. (1980), Sumino and Anderson (1984), Duffy and Anderson (1989), Bass and Kanzaki (1990), Leger et al. (1990), Yeganeh-Haeri et al. (1990), O'Neill et al. (1991), Armbruster et al. (1992), Rigden et al. (1994), Pacalo and Weidner (1997), Sinogeikin et al. (1997), Gwanmesia et al. (1998), Wang et al. (1998), Chen et al. (1999), Conrad et al. (1999), Zhang et al. (1999), Gwanmesia et al. (2000), Lui et al. (2000), Wang and Ji (2001), Sinogeikin and Bass (2002a,b), Gwanmesia et al. (2006).

the pressure and temperature increase. This changes the composition of the pyrope ($Mg_3Al_2Si_3O_{12}$)-rich garnet to give an increasing majorite ($Mg_4Si_4O_{12}$) content, by substituting Mg^{2+} and Si^{4+} onto the octahedral site, which is occupied by Al^{3+} in pyrope. As the majorite content of the garnet increases there is a corresponding decrease in the bulk and shear modulae (figures 1a and b).

Various authors (e.g. Cohen 1991, Gilman 2003) have argued that a material's bulk modulus is a good guide to its resistance to plastic deformation. Assuming that this is applicable in the garnet solid solution, majorite-rich garnets should be mechanically weaker than pyrope. The opposite conclusion is drawn by Karato et al. (1995) who argued that the strength of a range of low-pressure garnet-structured materials is a function of homologous temperature and normalised creep strength; they argue that majorite garnet should follow the same trend and will therefore be stronger than pyrope in the transition zone. Kavner et al. (2000) find that majorite supports a larger shear stress than pyrope in room temperature diamond-anvil cell studies, consistent with the conclusions of Karato et al. (1995); however, no high temperature studies of majorite strength or rheology have previously been reported.

We have performed relative-strength experiments to resolve the conundrum as to whether majoritic garnets are stronger or weaker than pyrope, as well as to generate sufficient data to calculate a flow law for more majorite-rich garnets. The relative strength experiments were undertaken on beam line X17B2 at the NSLS, Brookhaven National Laboratory, USA.

2. Experimental method

This section has been divided in to two parts during revision; the tow parts are now experimental method and data analysis. The experimental method section contains the

information about how the experiments were performed; and is equivalent to lines 39 to 73 in the unrevised text.

The relative-strength experiments reported here were performed on beamline X17B2 at the NSLS (Weidner et al. 1992), using both the Deformation-DIA (D-DIA; Wang et al. 2003) and T-Cup (Vaughan et al. 1998) multi-anvil press modules in a 200 tonne load frame. The detector arrangement of this beamline consisted of four energy-dispersive detectors aligned in pairs to observe the diffraction patterns from the samples both parallel and perpendicular to the direction of uniaxial deformation. This is sufficient to constrain the hydrostatic and differential stress on the sample because the sample geometry is axi-symmetric. The diffraction detectors are complimented by a fluorescent YAG crystal and visible light CCD camera which image the sample during the experiment. Each experiment contained two samples which were stacked on top of each other and then deformed simultaneously under near-identical conditions; such an experimental design has been used previously (e.g. Li et al. 2003, 2006, Hunt et al. 2009).

The first experiment in this study was performed in a 6/4 D-DIA cell to investigate the relative strength of pyrope and $py_{95}mj_5$ as a function of temperature; the cell design for this experiment is illustrated in figure 2a. This was followed by experiments in the T-Cup to investigate the relative strength of more majoritic garnets (which would exolve enstatite at the lower pressures attainable in the D-DIA) and pyrope in stress relaxation experiments. The T-Cup experiments had pairs of samples with compositions of pyrope with 75 % pyrope ($py_{75}mj_{25}$), and 75 % pyrope with 50 % pyrope ($py_{50}mj_{50}$); an experiment with a pure majorite sample was attempted but the majorite transformed to enstatite. The successful T-Cup experiments were undertaken in 7/3 and 7/2 cells respectively; the cell design for both experiments was the same and is illustrated in figure 2b. The majorite-containing starting samples were made from synthetic end-member pyrope (py_{100}) and majorite (mj_{100}) glasses which were mixed then repeatedly glassed in air at 1600 °C and ground under acetone until homogeneous. These glasses were then transformed into garnets at pressure and approximately 1400 °C in a 1000 tonne multi-anvil press at UCL; the recovered products were analysed by X-ray diffraction to confirm their crystal structure and phase purity. The recovered samples were ground for use as starting materials in the deformation experiments.

Each deformation experiment was conducted as follows. Prior to compression of the sample diffraction patterns were acquired from each sample in the cell for the measurement of a reference unit cell volume, V_0. The sample assembly was then compressed at room temperature to the required end load at which point an X-radiograph and diffraction patterns from each sample were recorded. The cell was then heated to the desired temperature, and for the D-DIA experiment the active deformation was started; there was no annealing before deformation to remove compression damage. The elastic and macroscopic strains were observed throughout the experiment by the acquisition of a repeated sequence of alternate radiography and diffraction measurements. The exposure time of the images was of the order of tens of microseconds, and the time taken to collect each diffraction pattern was approximately 5 minutes. The

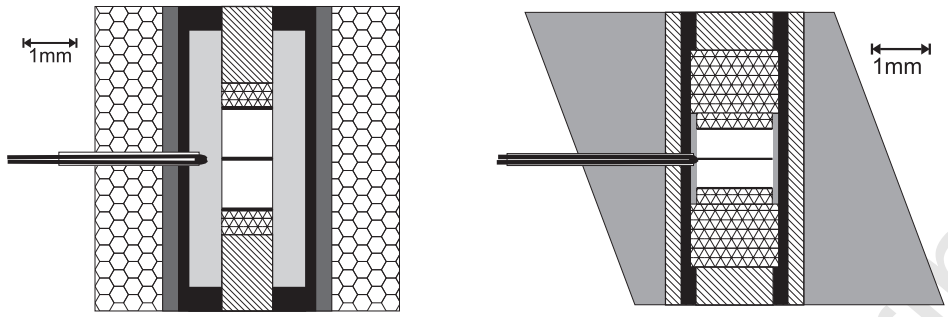

(a) 6/4 D-DIA cell **(b)** 7/3 T-Cup cell

Figure 2: A schematic of the D-DIA cell and a example of the T-Cup cell used at the NSLS in this study. The hexagons are the boron epoxy cube for the D-DIA cell, the dark grey – MgO, black – graphite, light grey – boron nitride, triangles – Al_2O_3 pistons, hatching – crushable alumina, heavy black lines are foil markers between the samples which are white.

temperature was increased when either: a few percent strain had been accumulated in the samples under the current conditions or, in the stress-relaxation experiments, the samples had stopped straining.

3. Data analysis

This is a new section which describes all the data analysis performed on the data in this study. It contains the method we used to calculation the stress and plastic strain in the samples (lines 80 - 130 in unrevised manuscript) along with the analysis for deriving the flow law (lines 196 - 205 in unrevised manuscript). There are additionally a number of other changes requested by the reviewers, for example an expanded explanation of how the stresses are calculated from the diffraction patterns.

Diffraction patterns were analysed for phases present and unit cell parameter using plot85 and the axial and radial elastic strains calculated. Calculation of the elastic strains requires the thermal expansion of the samples; the value taken for the volumetric thermal expansion was that of pyrope ($19.9 \times 10^{-6}\,\mathrm{K}^{-1}$; Fei 1995) and was assumed to be independent of pressure, temperature and composition. The stresses can then be calculated, for an aggregate of randomly orientated cubic polycrystals in an axi-symmetric stress field (Nye 1985, page 143):

$$\sigma_a = c_{11}\varepsilon_a + 2c_{12}\varepsilon_r \tag{1a}$$

$$\sigma_r = c_{11}\varepsilon_r + c_{12}(\varepsilon_a + \varepsilon_r) \tag{1b}$$

where σ_a and σ_r are the stresses in the axial and radial directions respectively, ε_a and ε_r are the crystallographic strains in the same directions. The values c_{11} and c_{12} are the elastic constants (generically c_{ij}) for the samples, at the conditions of the measurement; no averaging of the elastic constants is needed because garnet is cubic.

	Continuous composition derivatives		Discontinuous composition derivatives			
	All majorite contents		High majorite ($X_{\mathrm{mj}} > 0.67$)		Low majorite ($X_{\mathrm{mj}} \leqslant 0.67$)	
	Value at $X_{\mathrm{mj}} = 0$	$\partial/\partial X_{\mathrm{mj}}$	Value at $X_{\mathrm{mj}} = 0$	$\partial/\partial X_{\mathrm{mj}}$	Value at $X_{\mathrm{mj}} = 0$	$\partial/\partial X_{\mathrm{mj}}$
K	172.9 ± 0.3	-10.9 ± 0.7	168.9 ± 5.5	-6.7 ± 6.0	172.9 ± 0.3	-10.9 ± 0.7
μ	91.6 ± 0.2	-3.7 ± 0.3	81.4 ± 2.7	7.3 ± 2.9	91.7 ± 0.2	-4.7 ± 0.8

Table 1: Composition dependencies of $K_{X_{\mathrm{mj}}}$ and $\mu_{X_{\mathrm{mj}}}$ on majorite content, where $X_{\mathrm{mj}} = [\mathrm{mj}]/([\mathrm{mj}] + [\mathrm{py}])$. The numbers presented here are those that describe the fits in figures 1a and b. The units of the intercept values and slopes are GPa and GPa/X_{mj} respectively.

The c_{ij} values used in this study are taken to change as a function of pressure, temperature and majorite content, according to the relationship:

$$c_{ij}^{P,T,X_{\mathrm{mj}}} = c_{ij}^{0} + P\frac{\partial c_{ij}}{\partial P} + T\frac{\partial c_{ij}}{\partial T} + X_{\mathrm{mj}}\frac{\partial c_{ij}}{\partial X_{\mathrm{mj}}} \tag{2}$$

where P is the pressure, T is the temperature, c_{ij}^{0} are the c_{ij} values of pure pyrope at room pressure and temperature. X_{mj} is the majorite content of the garnet, which as is defined as:

$$X_{\mathrm{mj}} = \frac{[\mathrm{mj}]}{[\mathrm{mj}] + [\mathrm{py}]} \tag{3}$$

and [mj] and [py] are the molar proportions of majorite and pyrope in the samples.

The c_{ij}^{0} values and their composition derivatives ($\partial c_{ij}/\partial X_{\mathrm{mj}}$) have been derived (using Lamé's relationships, e.g. Poirier 2000, pages 13-14) from a weighted fit to values of the bulk (K) and shear (μ) modulae for the pyrope–majorite solid solution taken from the literature (figure 1). The dependency of c_{ij} with majorite content ($\partial c_{ij}/\partial X_{\mathrm{mj}}$) and the value for pure pyrope (c_{ij}^{0}) can be interpolated from the published data by assuming either that the composition dependency is continuous (solid lines, figure 1) or that there is a discontinuity in the composition dependency (dashed lines, figure 1). A discontinuity in $\partial K/\partial X_{\mathrm{mj}}$ and $\partial \mu/\partial X_{\mathrm{mj}}$ is preferred by Sinogeikin et al. (1997) on the basis that a cubic-tetragonal transition occurs in pyrope–majorite garnets at ambient conditions and $X_{\mathrm{mj}} = 0.67$. However, they could not exclude the possibility that the modulae decrease continuously across the solid solution. Heinemann et al. (1997) concluded that the cubic-tetragonal transition in pyrope–majorite garnets, a likely source for any discontinuity in the composition derivative, does not occur at high pressures and temperatures in majorite rich garnets. Therefore, in the present study, the composition derivatives of the moduli are considered to be continuous across the entire solid solution, particularly since the composition of the present samples were less than $X_{\mathrm{mj}} = 0.5$. The weighted least-squares fits to the data giving the changes in K and μ as a function of majorite content in pyrope, both with and without a discontinuity, are presented in table 1; the data which were published without errors have been left out of the analysis, although they are included in figure 1.

Measurements of the pressure derivatives of K and μ ($\partial K/\partial P$ and $\partial \mu/\partial P$) as a function of majorite content are not as numerous as measurements of merely the modulae; the papers which include pressure dependency data are: Duffy and Anderson (1989), Rigden et al. (1994), Gwanmesia et al. (1998), Wang et al. (1998), Chen et al. (1999), Lui et al. (2000), Wang and Ji (2001), Sinogeikin and Bass (2002a), Gwanmesia et al. (2006). There is no definitive composition dependency to the pressure derivatives of

c_{ij}	$c_{ij,X_{\mathrm{mj}}=0}$ (GPa)	$\frac{\partial c_{ij}}{\partial P}$	$\frac{\partial c_{ij}}{\partial T}$ (GPa K^{-1})	$\frac{\partial c_{ij}}{\partial \%\mathrm{Mj}}$ (GPa $X_{\mathrm{mj}}{}^{-1}$)
c_{11}	295.0 ± 0.3	6.9 ± 0.1	-0.033 ± <0.001	-16.4 ± 0.9
c_{12}	111.8 ± 0.5	3.5 ± 0.1	-0.013 ± <0.001	-72.0 ± 1.2
c_{44}	91.6 ± 0.2	1.8 ± 0.1	-0.010 ± <0.001	-37.0 ± 0.3

Table 2: Table of the isotropic c_{ij} values used in this study to calculate the stresses in the garnet samples from the elastic strains. For details of the origin of the numbers see text; the data from which these data are derived are listed in the caption for figure 1.

c_{ij} demonstrated by these data and therefore the pressure derivatives are calculated as a weighted fit to the published $\partial K/\partial P$ and $\partial \mu/\partial P$ values assuming that there is no composition dependence. The temperature derivatives of the c_{ij} values ($\partial c_{ij}/\partial T$) are isotropic Hill averages of the single crystal data for the 'pyrope-rich garnet' in Anderson and Isaak (1995); they are also assumed to be independent of composition. All other higher order derivatives are assumed to be negligible. A summary of the c_{ij} values and their derivatives used in this study is presented in table 2.

The change in the length of the samples throughout the experiment was calculated, from the radiographs, by the cross-correlation method described previously by Li et al. (2003). From these length changes the sample strains can be calculated, the errors of which are estimated assuming that; (1) there is a 5 pixel error in the starting length of the sample, and (2) the error in length change between two adjacent images is 0.05 pixels. This radiographically measured strain ($\Delta l/l_0$) contains a recoverable elastic strain component, as well as a component due to unrecoverable plastic strain. During deformation at constant stress and temperature (in the D-DIA) the elastic strain is constant and the plastic strain-rate is equal to the observed bulk strain-rate. This is not the case for stress-relaxation experiments (in the T-Cup) where both the elastic and plastic strains vary simultaneously; consequentially the strain-rates measured by radiography are not necessarily equal to the true plastic strain-rates in the samples. Therefore, to calculate the instantaneous plastic strain-rates we first calculate the true instantaneous plastic-strains using the procedure of Durham et al. (2002), who define the plastic strain developed during some time interval as:

$$\varepsilon = \frac{R_{k,n} - R_{k,n+1}}{R_{k,n}} \tag{4a}$$

where R_k is the so called Kung ratio:

$$R_k = \frac{l_n}{l_0} / \frac{a_n}{a_0} \tag{4b}$$

The sample length is l, a is the axial unit-cell length measured by diffraction and the subscript n denotes the values at time n. The ratio R_k is the compliment of the bulk strain which would be observed if the sample was instantly relaxed to zero stress and room temperature at the time of the measurement.

In order to calculate R_k properly the values of a and l need to be coincident in time, which in the raw data they are not. Therefore, the axial crystallographic length (a in equation 4b) was calculated at the time of the radiography measurements by interpolation. The plastic strains and instantaneous

strain-rates were then calculated from R_k for each sample. The ratios of the instantaneous strain-rates from the T-Cup and D-DIA experiments were then used to determine the effect of temperature and composition on the strength of the garnet solid-solution.

The experimental data in this study were not sufficiently constrained or abundant to determine independent flows law for pyrope-majorite garnets. However, with some manipulation, the ratio of the strain-rates of the pyrope and majoritic samples can be used to derive a flow law for majorite-containing garnets relative to the flow law for pure pyrope. This relative flow law can then be combined the with flow laws of previous studies on pure pyrope (Dobson et al. 2005, Li et al. 2006) to give a flow law for the entire pyrope–majorite solid solution, which is important for mantle garnet compositions. The flow law for majoritic garnet relative to that for pyrope is derived from the flow laws for the two separate phases as follows. We assume a generic flow-law for plastic deformation of:

$$\dot{\varepsilon} = A_0 \sigma^n \exp\left(\frac{-Q}{RT}\right) \tag{5}$$

where $\dot{\varepsilon}$ is the strain rate, A_0 is the pre-exponential factor, σ the differential stress, n the stress exponent, Q is the activation energy for creep, R the gas constant and T the absolute temperature; this is the flow-law generally applied to climb-assisted dislocation glide deformation. Rearranging this equation for Q and taking the difference between the two relationships for majoritic and pyrope garnets gives the difference between the activation energies of majoritic and pyrope garnet:

$$Q^{X_{\mathrm{mj}}} - Q^{\mathrm{py}} = -\frac{(\log \dot{\varepsilon}^{X_{\mathrm{mj}}} - \log A_0^{X_{\mathrm{mj}}} - n^{X_{\mathrm{mj}}} \log \sigma) - (\log \dot{\varepsilon}^{\mathrm{py}} - \log A_0^{\mathrm{py}} - n^{\mathrm{py}} \log \sigma)}{\frac{1}{\mathrm{R}T}} \tag{6}$$

where the superscripts 'X_{mj}' and 'py' denote the majorite- and pyrope-rich phases respectively. Under the experimental conditions the stresses in both the samples are the same and assuming that the stress dependency does not change as a function of majorite content (*i.e.* $n^{X_{\mathrm{mj}}} = n^{\mathrm{py}}$) the stress dependencies cancel. By also assuming that the A_0 values have no temperature dependency, which is true for a simple Arrhenius process, the equation above simplifies to:

$$\begin{aligned} Q^{X_{\mathrm{mj}}} - Q^{\mathrm{py}} &= -\left[\frac{\partial(\log \dot{\varepsilon}^{X_{\mathrm{mj}}} - \log \dot{\varepsilon}^{\mathrm{py}})}{\partial \frac{1}{\mathrm{R}T}}\right]_\sigma \\ &= -\left[\frac{\partial \log(\frac{\dot{\varepsilon}^{X_{\mathrm{mj}}}}{\dot{\varepsilon}^{\mathrm{py}}})}{\partial \frac{1}{\mathrm{R}T}}\right]_\sigma \end{aligned} \tag{7}$$

It is therefore possible to calculate the differences in activation energy and pre-exponential factors for high-temperature creep in pyrope and majoritic garnets.

The activation energy (Q) can be split into two parts: the activation enthalpy (E^*) and an activation volume (V^*):

$$Q = E^* + PV^* \tag{8}$$

where P is the pressure. If the activation volumes for pyrope and majoritic garnets are identical the activation energy (Q) in equation 7 is independent of pressure because the PV^*_{py} and $PV^*_{X_{\mathrm{mj}}}$ terms cancel. For the experiments conducted here, no correlation between the strain-rate ratios and the measured

	Run #	Samples	T (°C)	P (GPa)	σ (GPa)	$\dot{\bar{\varepsilon}}_{X_{mj}}$ ($\times 10^{-6}s^{-1}$)	$\dot{\bar{\varepsilon}}_{py}$ ($\times 10^{-6}s^{-1}$)	Ratio ($\dot{\varepsilon}_{X_{mj}}/\dot{\varepsilon}_{py}$)
D-DIA	Garn_33	$py_{95}mj_5$	800	9.2 ± 0.2	1.4 ± 0.1	2.05 ± 0.05	2.38 ± 0.05	0.86 ± 0.03
		py_{100}	1000	8.7 ± 0.1	1.4 ± 0.1	4.99 ± 0.04	5.05 ± 0.03	0.98 ± 0.01
			1200	7.9 ± 0.1	1.4 ± 0.1	6.85 ± 0.06	6.13 ± 0.04	1.12 ± 0.01
T-Cup	Garn_35	$py_{75}mj_{25}$	500	9.5 ± 0.2	2.4 ± 0.1	3.2 ± 1.2	2.3 ± 0.8	1.38 ± 0.41
		py_{100}	600	11.4 ± 0.1	1.0 ± 0.1	4.7 ± 1.5	8.1 ± 2.6	0.58 ± 0.14
			775	13.3 ± 0.1	0.4 ± 0.1	11.7 ± 1.3	14.9 ± 1.5	0.78 ± 0.06
			850	13.6 ± 0.1	0.2 ± 0.1	4.4 ± 0.3	1.0 ± 0.2	4.65 ± 0.50
			900	12.5 ± 0.1	$< 0.1 \pm 0.1$	–	–	
	Garn_36	$py_{50}mj_{50}$	600	12.9 ± 0.2	2.5 ± 0.2	10.8 ± 2.6	11.5 ± 3.7	0.94 ± 0.22
		$py_{75}mj_{25}$	670	11.5 ± 0.2	0.5 ± 0.1	1.4 ± 0.3	8.9 ± 1.0	0.16 ± 0.02
			720	11.9 ± 0.2	0.2 ± 0.1	3.4 ± 0.4	7.5 ± 0.7	0.45 ± 0.04
			770	10.5 ± 0.1	$< 0.1 \pm 0.1$	3.2 ± 0.3	6.2 ± 0.4	0.51 ± 0.03
			920	7.6 ± 0.1	$< 0.1 \pm 0.1$	2.8 ± 0.2	0.8 ± 0.2	3.95 ± 0.60

Table 3: Strain rates and experimental conditions for the pyrope-majorite relative strength experiments. The strain-rates presented here for the Garn_35 and 36 are the arithmetic averages of the instantaneous strain-rates and as such are only included to give an indication of the actual strain-rates in the experiment; strain-rate ratios for the stress-relaxation experiments are the average of the instantaneous strain-rate ratio at those conditions. The data in this table have been plotted in figure 7.

pressure was discernible in the experimental data. Therefore, it has been assumed that the volume of activation is constant across the solid solution ($V^*_{py} = V^*_{X_{mj}}$) and has no effect on the strain-rate ratio.

4. Results

This is the section of the paper which has undergone the most changes. The discussion of how we derived the flow law has been moved to the *data analysis* section and the discussion of the three different experiments expanded as per the requests of the reviewers. Each experiment is now discussed separately. Two new figures have been added to the section showing the plastic strain in experiment 35 and images of the recovered samples. Furthermore, the strain-rate ratios and the derivation of the flow law for majorite garnets are now in separate subsections.

The three successful synchrotron experiments undertaken in this study were analysed to find the ratio of the strain-rates for the two samples during the experiment and the results are presented in table 3 as a function of temperature. The data were analysed in slightly different manners for the D-DIA (Garn_33) and T-Cup experiments but the data from the two T-Cup experiments (Garn_35 and 36) were analysed in an identical manner.

D-DIA experiment — py_{100}–$py_{95}mj_5$ (Garn_33)

The first experiment was undertaken in the D-DIA with samples of py_{100} and $py_{95}mj_5$ with constant strain-rates. The pressure and differential stresses during this experiment were constant at each set of conditions (table 3) and therefore it is possible to calculate the plastic-strains directly from the radiography images, rather than *via* the Kung ratio (equations 4a and 4b). Measured strains are plotted in figure 3.

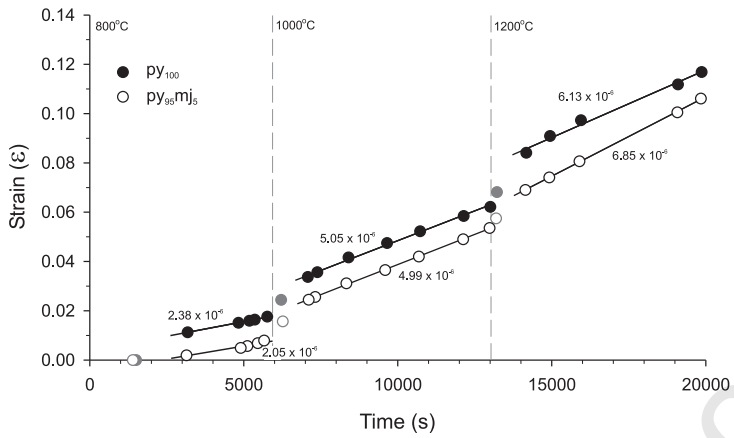

Figure 3: Strain as a function of time during experiment Garn_33. The filled symbols are for the py_{100} sample and the open symbols are the $py_{95}mj_5$ sample; the grey symbols indicate those data points not used in the calculation of the strain-rates; the first black point at each temperature was used as the l_0 in the strain calculation.

The sample strain-rates ($\dot{\varepsilon}_{X_{\mathrm{mj}}}/\dot{\varepsilon}_{\mathrm{py}}$) changes systematically with temperature (table 3). The first data point after heating (grey points in figure 3) were excluded from the strain-rate calculations in order to avoid including the transient effects that result from heating. The strain-rate ratio decreases with increasing temperature; at 800°C the $py_{95}mj_5$ garnet is weaker than pyrope but at 1200°C the reverse is true.

T-Cup experiments — py_{100}–$py_{75}mj_{25}$ (Garn_35) and $py_{75}mj_{25}$–$py_{50}mj_{50}$ (Garn_36)

Two stress-relaxation experiments were performed in the T-Cup, with higher majorite contents in the garnets and at higher pressure than the experiment in the D-DIA. To calculate the plastic component of the strains from these stress-relaxation experiments it was necessary to use the Kung ratio (equations 4a and 4b); the resulting plastic strains are plotted in figures 4a (Garn_35) and 5 (Garn_36). The plastic strains calculated in this way differ from the strains calculated directly from the radiography images by between 1 and 2 % with most of this difference occuring during initial heating of the samples.

The most significant feature of the plastic strain in Garn_35 (samples: py_{100} and $py_{75}mj_{25}$) is that there is a significant increase in the strain accommodated by both samples upon increasing the temperature from 600 to 775 °C. This temperature range is consistent with the weakening observed in garnets by Weidner et al. (2001). As with Garn_33, above 600 °C, there is a weakening of majorite-rich garnets relative to pyrope with increasing temperature.

The increase in strain with time during the experiment is more monotonic in Garn_36 than Garn_35 but similar features can be observed in the data. At 600°C the strain-rates are approximately the same, between 670 and 770°C the $py_{50}mj_{50}$ sample has a slower strain-rate than the more pyrope rich sample and at 900°C the $py_{75}mj_{25}$ sample almost stops straining, whist the $py_{50}mj_{50}$ continues to deform. Above 770°C in Garn_36 the differential stresses became too small to measure, but the samples continued to strain in a manner consistent with the rest of the experimental results. Moreover, at room temperature the more majorite-rich sample supported a higher differential stress (6.5 ± 0.4 GPa in the $py_{50}mj_{50}$

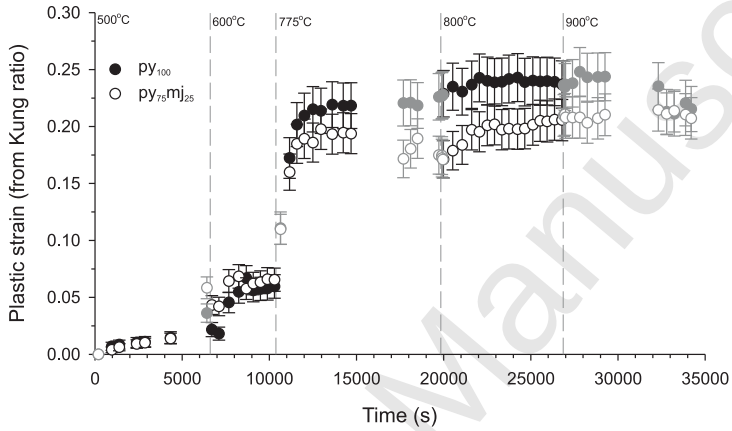

(a) Plastic strain (from R_k)

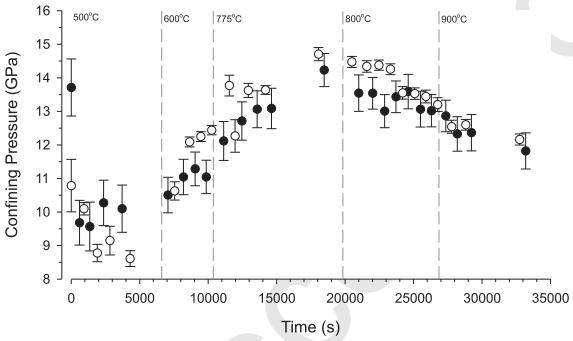

(b) Confining pressure

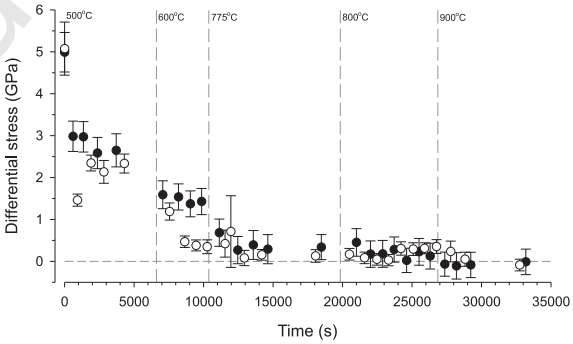

(c) Differential stress

Figure 4: Strain and stresses during experiment Garn_35. The filled symbols are for the py_{100} sample and the open symbols are the $py_{75}mj_{25}$ sample; the vertical dashed lines indicate the time at which the temperature was increased to the values adjacent to the lines. The grey symbols in part (a) indicate data points not used in calculating the ratios of the strain rates.

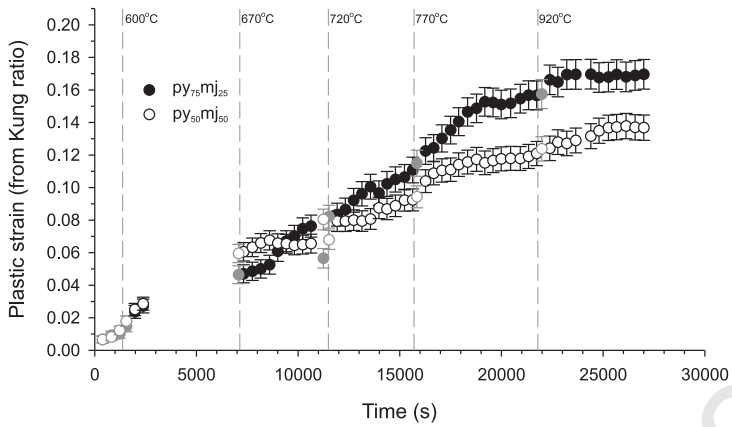

Figure 5: Strain and stresses during experiment Garn_36. The filled symbols are for the $py_{75}mj_{25}$ sample and the open symbols are the $py_{50}mj_{50}$ sample; the vertical dashed lines indicate the time at which the temperature was increased to the values adjacent to the lines. The grey symbols indicate data points not used in calculating the ratios of the strain rates.

sample as opposed to 1.7 ± 0.9 GPa in the $py_{75}mj_{25}$ sample). This is consistent with the observations of Kavner et al. (2000), who observed that majoritic garnets support a very large differential stress at room temperature.

The confining pressures throughout Garn_35 are high enough for the $py_{75}mj_{25}$ sample to be stable but in Garn_36 the pressures drop below the ≈12.8 GPa pressure required for the $py_{75}mj_{25}$ garnet to be in its stability field. At the temperatures of these experiments the kinetics of the decomposition reaction proved to be too slow for enstatite to form, indeed no enstatite peaks were observed in any of the diffraction patterns. We note here that a further experiment, Garn_37, was performed with pure majorite as one of the samples; this sample was observed to transform to pyroxene at ≈11.4 GPa and 550°C. For all the experiments, the difference between the pressures measured from the two samples were for the most part within two standard deviations of each other (figure 4b shows the pressures measured during Garn_35); the same is true for the differential stresses at high temperature (figure 4c – differential stresses from Garn_35). The mean pressures and differential stresses for each temperature in all the experiments are listed in table 3.

Recovered samples

Figure 6 presents two secondary electron images of the samples recovered from experiment Garn_36; these images are typical of the recovered samples from all the experiments reported here. In these images it can be observed that the grains are between 1 and 5 μm in size, with a mean of approximately 2 μm. the similarity of the grain-sizes between the two samples means that it is unlikely that the difference in strength between samples is due to crystal superplasticity.

Strain-rate ratios

The ratio of the instantaneous strain-rates of the two pairs of samples in each experiment were calculated (table 3) excluding the data highlighted in grey in figures 3, 4 and 5. These data have

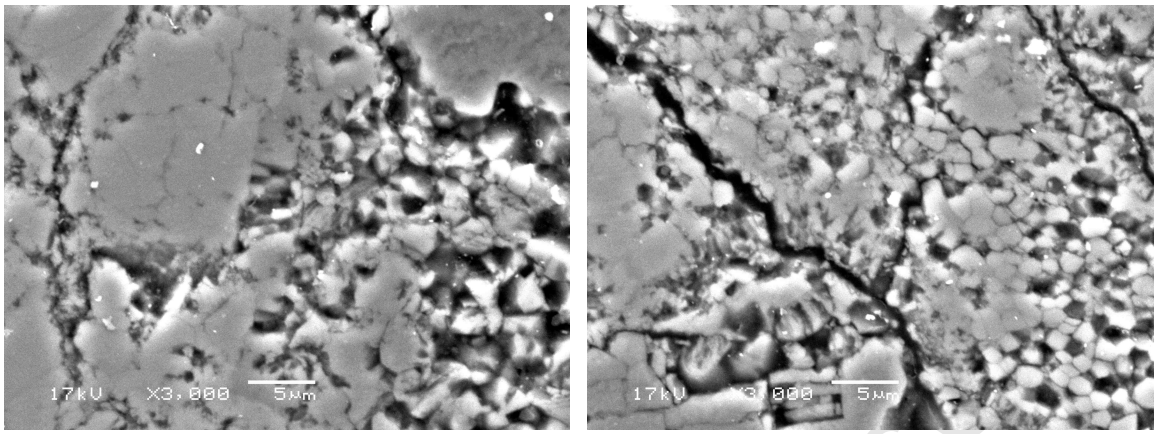

Figure 6: SEM micrographs of the recovered samples from experiment Garn_36; the left-hand image is of the $py_{75}mj_{25}$ sample and the right-hand image of the $py_{50}mj_{50}$ sample.

Experiment	Garn_33	Garn_35	Garn_36	35 & 36 combined
Sample 1	py_{100}	py_{100}	$py_{75}mj_{25}$	py_{100}
Sample 2	$py_{95}mj_{5}$	$py_{75}mj_{25}$	$py_{50}mj_{50}$	$py_{50}mj_{50}$
$Q^{X_{\mathrm{mj}}} - Q^{\mathrm{py}}$	3.9 ± 0.4	101.0 ± 7.4	57.1 ± 4.3	158.1 ± 8.5
$\log A_0^{X_{\mathrm{mj}}} - \log A_0^{\mathrm{py}}$	0.37 ± 0.03	11.48 ± 0.83	6.31 ± 0.49	17.79 ± 0.96

Table 4: Activation energy differences and A_0 values for the pyrope–majorite experiments. These fits are the lines that are plotted in figure 7.

been excluded because either they are immediately after heating of the samples and so will incorporate transient effects or the sample is not straining significantly under the conditions. The resulting ratios are plotted in figure 7. The most obvious feature in this graph is the change in behaviour above and below ≈ 650°C ($1/\mathrm{R}T \approx 1.30 \times 10^{-4}$ mol J^{-1}). Below 650 °C the strain-rate ratio measurements show no strong temperature dependency and the mean value (0.97 ± 0.16) is within error of unity, whilst above 650°C there is a clear temperature dependency. In Garn_35 and 36, above 800°C the more majoritic samples are weaker (i.e. straining faster) than the pyrope samples, whereas between 650 and 770°C the pyrope-rich samples are weaker. The D-DIA experiment (Garn_33) follows a similar pattern however the majoritic sample is weaker above 1050°C and stronger below this temperature.

The temperature at which the strain-rate ratios change from being temperature independent to temperature dependant is about 650°C. This is within the temperature range for the change in deformation mechanism from dislocation glide to climb-assisted dislocation glide (after Dobson et al. 2005), and approximately the temperature above which cation diffusion in metamorphic garnets becomes significant (Yardley 1977). Moreover, around this temperature, depending on the strain rate, there is a change in the microstructure of both naturally and experimentally deformed garnets (Voegelé et al. 1998a,b).

Above 650°C the strain-rate ratios become sensitive to temperature and at these temperatures climb-assisted dislocation glide is the dominant deformation-mechanism (Li et al. 2006). Between 650 and 800°C majoritic garnets are stronger than pyrope; however, this does not mean that there is an increase in the absolute strength of majoritic garnets but only that the majorite phase has weakened less than

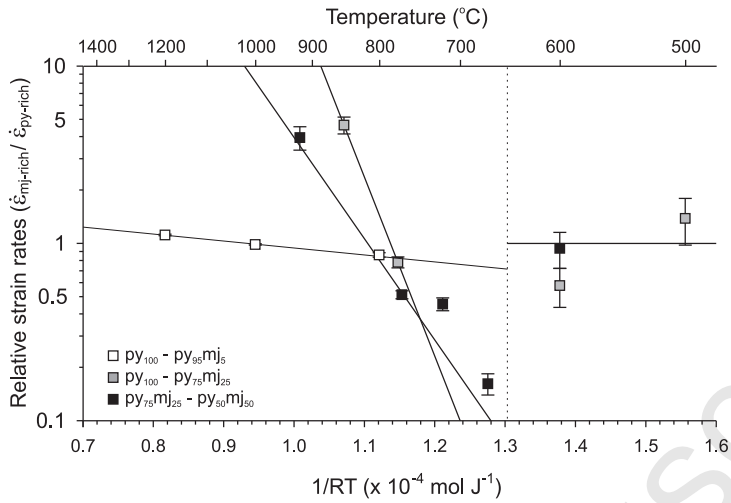

Figure 7: Ratio of the strain-rates in the pyrope and py-mj samples against 1/RT for experiments in this study, where T is the absolute temperature. The vertical dotted line is the approximate temperature at which the deformation mechanism changes from dislocation glide to climb and the errors of the offline experiments have been omitted because of their size. The data plotted here is presented in table 3 and the weighted fits to the data are presented in table 4.

the pyrope as the deformation mechanism changes from dislocation glide to climb-assisted glide, indeed there is a 10-fold weakening in Garn_35 between 600 and 750°C. The strain-rate ratios of the py_{100}–$py_{95}mj_5$ experiment show a smaller temperature dependence than the other experiments which have a 25 %-majorite difference between the samples and the $py_{75}mj_{25}$–$py_{50}mj_{50}$ has a lower dependency on temperature than the py_{100}–$py_{75}mj_{25}$ experiment.

Flow-law for majorite containing garnets

From the strain-rate ratios (figure 7, table 3) the activation energy (Q) of majoritic garnets relative to that of pyrope has been calculated, using equation 7. These activation energy differences, calculated from a weighted fit to each set of experimental data above 650°C, are presented in table 4; the differences between the logarithms of pre-exponential factors ($\log A_0$) are also included in the table. In the final column in table 4 the values from experiments Garn_35 and 36 are summed to give the differences in activation energy and logarithms of the pre-exponential factors between pyrope and $py_{50}mj_{50}$.

From these activation energy differences the change in activation energy as a function of majorite content across the entire pyrope-majorite solid solution can be derived assuming that the cubic–tetragonal transition does not have a significant effect on rheology or that it does not occur at elevated pressures and temperatures (after Heinemann et al. 1997). The activation energy differences between pyrope and majoritic garnets have been plotted as a function of X_{mj} in figure 8.

The functional form of the activation energy difference between pyrope and majoritic garnets is not known and no previous work has been found in which the expected functional form has been derived. However, there are various constraints on the function which the relationship must have beyond the values of the data. The function $Q^{X_{\mathrm{mj}}} - Q^{\mathrm{py}}$ must be zero at $X_{\mathrm{mj}} = 0$. For both 'low' and 'high' majorite contents there is expected to be relatively little change in the activation energy for creep as

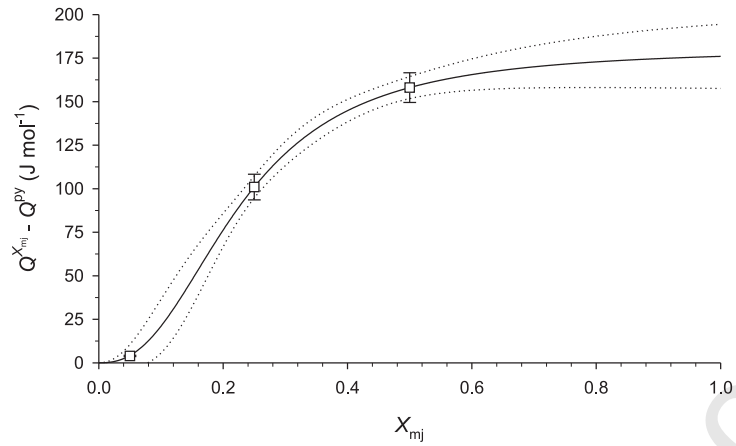

Figure 8: Activation energy difference for the pyrope–majorite solid-solution as a function of majorite content in the high temperature regime (T> 650°C); the solid line is the fit to the data defined by equation 9c and the dashed lines are one the standard error boundaries of the fit. The errors on the data points are the weighted fits presented in table 4.

a function of X_{mj} because the occupancy of the octahedral site will be dominated by Al^{3+} or Si^{4+} and Mg^{2+} respectively. Most of the change in activation energy will therefore be at at 'intermediate' compositions, but what constitutes 'low', 'intermediate' and 'high' compositions is not known *a priori*. These constraints define the activation energy to be a sigmoidal function of majorite content. The best fitting function (solid line in figure 8) was found to be an asymmetric sigmoid and has the form:

$$Q^{X_{\mathrm{mj}}} - Q^{\mathrm{py}} = a\left(\frac{b \cdot {X_{\mathrm{mj}}}^{c}}{1 + b \cdot {X_{\mathrm{mj}}}^{c}}\right)$$

where a, b and c are constants.

This relationship has the same form as the Hill equation (Hill 1910, who used it to describe oxygen ligand bonding to haemoglobin). Significantly however, this function passes through zero at no majorite content and has by far the lowest least squares misfit of all the functions tried. Moreover, the function does not asymptote with increasing majorite content. The sparsity of the data and the errors on the activation energy differences do not preclude the possibility that the actual functional form of the relationship is different from that used here. A similar analysis has been performed for the value of the pre-exponential factor difference assuming that both pyrope and majorite have the same stress dependencies and, again, the Hill equation has the smallest least squares residual of all the functions tried.

Combined, these relationships define the flow law for majoritic garnets relative to that of pyrope to be:

$$\dot{\varepsilon}_{X_{\mathrm{mj}}} = \begin{cases} \dot{\varepsilon}_{\mathrm{py}} & \text{when } T < 650°\mathrm{C}, \\ A_0^{X_{\mathrm{mj}}} \sigma^n \exp\left(\frac{-Q^{X_{\mathrm{mj}}}}{\mathrm{R}T}\right) & \text{when } T \geqslant 650°\mathrm{C}. \end{cases} \tag{9a}$$

where

$$\log A_0^{X_{\mathrm{mj}}} = \log A_0^{\mathrm{py}} + 19.9(13)\left(\frac{51.8(489)\cdot {X_{\mathrm{mj}}}^{2.6(6)}}{1+51.8(489)\cdot {X_{\mathrm{mj}}}^{2.6(6)}}\right) \tag{9b}$$

$$Q^{X_{\mathrm{mj}}} = Q^{\mathrm{py}} + 180.5(119)\left(\frac{39.1(319)\cdot {X_{\mathrm{mj}}}^{2.5(5)}}{1+39.1(319)\cdot {X_{\mathrm{mj}}}^{2.5(5)}}\right) \tag{9c}$$

For reference the flow law for pyrope at less than 650°C has been measured by Dobson et al. (2005) and at greater than 650 °C by Li et al. (2006) who measured $Q^{\mathrm{py}} = 270 \pm 40\,\mathrm{kJ\,mol^{-1}}$ and $A_0^{\mathrm{py}} = 3.5^{+4.8}_{-2.0} \times 10^6 \mathrm{s}^{-1}$. Therefore the activation energy for climb-assisted dislocation glide in end-member majorite according to this study is $446 \pm 44\,\mathrm{kJ\,mol^{-1}}$.

5. Discussion

This section has only undergone minor changes from the unrevised version of the text. In the interests of readability, however, the section has been divided into two subsections which discuss the mineral physics and the implications for the mantle separately.

Mineral physics

The relationship between the strength of pyrope and majoritic garnets is more complex than initially expected. A change in relative strength with composition was expected but the temperature effect was not; in hindsight perhaps it should have been. Such temperature dependant behaviour has not been predicted previously but we are confident that the temperature effects observed here are robust and not an artefact derived from pressure effects. If all the experiments saw a reduction in sample pressure with increasing temperature we would be unable to distinguish between a pressure and temperature dependant rheology. However we saw the same temperature-dependent trend of strength in all experiments despite the pressure increasing slightly (Garn_35), dropping slightly (Garn_33) and dropping significantly (Garn_36). This suggests that the pressure effect is small, supporting our neglect of the PV^* term, in equation 8.

The change in strength between pyrope and majoritic garnets is clear to see in figure 7. At low temperatures (< 650°C) majoritic garnets have the same flow law as pyrope while at higher temperatures the flow law of majoritic garnets is significantly dependent on the majorite content of the garnet and the temperature (equation 9). The flow law derived here is consistent with a change in deformation mechanism in both pyrope and majoritic garnets at about 650°C. This is in agreement with the studies of Yardley (1977), Voegelé et al. (1998a,b), Dobson et al. (2005) among others, all of whom make arguments related to a change in deformation mechanism at about this temperature.

The relative flow-law presented here, in equation 9, is valid assuming that the stress dependences (n) of pyrope and majoritic garnets are the same. In the calculation for the flow-law if they are the same they cancel but if not the pre-exponential factor as formulated here has a stress dependant term in it. It cannot, however, be discerned from this data set if there is a change in n with majorite composition.

We suggest the observed composition dependence of majorite rheology might be explained as follows: strain-rate, under a given differential stress, in the dislocation-climb regime is controlled by diffusion

of the chemical species. By adding Si onto the nominal 3+ site in garnet it becomes easier to create cation vacancies by local charge-balancing with Si^{4+}, increasing the vacancy concentration. This, in turn, increases the the pre-exponential factor in the strain-rate Arrhenius equation (equation 9b). However, adding silicon to the 3+ site also increases the migration enthalpy, resulting in an increase in the magnitude of the exponential term; hence the steeper gradients in figure 7 as a function of increasing majorite content. These two effects combine such that at temperatures above approximately 800°C highly majoritic garnets are weaker than pyrope.

Rheology of the mantle

In normal mantle, i.e. away from subduction zones, the highest garnet component of the mineralogy is in the transition-zone, at depths of about 520 km (Ringwood 1991), where the temperatures are between 1600 and 1700°C. At these conditions, majoritic garnets in the transition zone will be much weaker than pure pyrope would be at the same conditions. This, combined with the increased strength of the high pressure polymorphs of olivine (e.g. Weidner et al. 2001) relative to that of olivine, shows that majoritic garnets will be the weak phase in the transition zone; a conclusion which is contrary to the predictions of Karato et al. (1995) and Kavner et al. (2000).

Thermal models show that at transition zone depths the top-most layer of the subducting slab is at temperatures in excess of 800°C. Therefore any majoritic garnets in the MORB layer of the subducting slab will be weaker than if they were pure pyrope. Relative to the core of the slab, the MORB layer will be weaker because of the elevated temperatures and the weakening caused by the majorite component of the garnet. However, the weakening effect of majorite is unlikely to be sufficient to make the MORB layer weaker than the surrounding, non-subducting mantle because of the significant difference in temperature between the normal mantle ($T \approx 1600-1700$°C) and the top of the slab. Therefore, it is unlikely that this study invalidates previously published models of MORB layer delamination at the 660 km discontinuity (e.g. van Keken et al. 1996) but the relative viscosity of the garnet layer and the core of the subducting slab will be significantly reduced or even reversed and the models will need to be reassessed.

6. Summary and Conclusions

This is a new section to the paper which summarises the discivaries and lists our conclusions, as per the request of the reviews.

In this study we have measured the relative strength of garnets in the pyrope–majorite solid solution and shown that the strength of majorite relative to that of pyrope changes as a function of temperature and composition. A flow law for majorite has been enumerated (equation 9) and we conclude that the the activation energy for climb-assisted dislocation glide in end-member majorite is $446 \pm 44\,\mathrm{kJ\,mol^{-1}}$. At temperatures below 650 °C both pure pyrope and majoritic garnets have the same strength whilst above 650 °C we find that majoritic garnets are initially stronger than pure pyrope but weaken with increasing temperature and majorite content.

Furthermore, it has been shown here that using relative strength experiments the flow law for an entire solid solution can be determined from just a few experiments. Also in these experiments a flow law for iron-free majorite garnet has been determined without the need to perform experiments on pure majorite. This is therefore a potentially useful method to determine the flow laws of high pressure phases from the lower-pressure end of the solid solutions of which they are part.

Acknowledgements

We acknowledge funding from the following sources: EU, Marie Curie Fellowships contract HPMT-CT-2001-00231 (SAH), NERC (SAH, DPD), The Royal Society (DPD) and NSF grant EAR0809397 (LL). This research has been supported by a Marie Curie Fellowship of the European Community programme "Improving Human Research Potential and the Socio-economic Knowledge Base" under contract number HPMT-CT-2001-00231. Use of the National Synchrotron Light Source, Brookhaven National Laboratory, was supported by the U.S. Department of Energy, Office of Science, Office of Basic Energy Sciences, under Contract No. DE-AC02-98CH10886. We acknowledge two anonymous referees for their helpful comments which significantly improved the manuscript.

References

Anderson, D. L., Isaak, D. G., 1995. Elastic constants of mantle minerals at high temperature. In: Ahrens, T. J. (Ed.), Mineral Physics and Crystallography: A Handbook of Physical Constants. American Geophysics Union, pp. 64 – 97.

Armbruster, T., Geiger, C. A., Lager, G. A., 1992. Single-crystal X-ray structure study of synthetic pyrope almandine garnets at 100 and 293 K. American Mineralogist 77, 512 – 521.

Bass, J. D., Kanzaki, M., 1990. Elasticity of a majorite–pyrope solid solution. Geophysical Research Letters 17 (11), 1989 – 1992.

Chen, G., Cooke, J. A., Gwanmesia, G. D., Liebermann, R. C., 1999. Elastic wave velocities of $Mg_3Al_2Si_3O_{12}$-pyrope garnet to 10 GPa. American Mineralogist 84, 348 – 388.

Cohen, M. L., 1991. Predicting new solids and their properties. Philosophical Transactions of the Royal Society of London. Series A, Mathematical and Physical Sciences 334, 501 – 513.

Conrad, P. G., Zha, C.-S., Mao, H.-k., Hemley, R. J., 1999. The high-pressure, single-crystal elasticity of pyrope, grossular, and andradite. American Mineralogist 84, 374 – 383.

Dobson, D. P., Mecklenburgh, J., Alfe, D., Wood, I. G., Daymond, M. R., 2005. A new belt-type appratus for neutron-based rheological measurements at Gigapascal pressures. High Pressure Research 25 (2), 107 – 118.

Duffy, T. S., Anderson, D. L., 1989. Seismic velocities in mantle minerals and the mineralogy of the upper mantle. Journal of Geophysical Research 94 (B2), 1895 – 1912.

Durham, B., Weidner, D. J., Karato, S., Wang, Y., 2002. New developments in deformation experiments at high pressure. In: Karato, S., Wenk, H.-R. (Eds.), Plastic deformation of minerals and rocks. Vol. 51 of Reviews in mineralogy and geochemistry. Mineralogical Society of America, pp. 21 – 49.

Fei, Y., 1995. Thermal expansion. In: Ahrens, T. J. (Ed.), Mineral Physics and Crystallography: A Handbook of Physical Constants. American Geophysics Union, pp. 29 – 44.

Gilman, J. J., 2003. Electronic Basis of the Strength of Materials. Cambridge University Press, Cambridge, UK.

Gwanmesia, G. D., Chen, G., Liebermann, R. C., 1998. Sound velocities in $MgSiO_3$-garnet to 8 GPa. Geophysical Research Letters 25 (24), 4553 – 4556.

Gwanmesia, G. D., Lui, J., Chen, G., Kesson, S., Rigden, S. M., Liebermann, R. C., 2000. Elasticity of the pyrope ($Mg_3Al_2Si_3O_{12}$) – majorite ($MgSiO_3$) garnets solid solution. Physics and Chemistry of Minerals 27, 445 – 452.

Gwanmesia, G. D., Zhang, J., Darling, K., Kung, J., Li, B., Wang, L., Neuville, D., Liebermann, R. C., 2006. Elasticity of polycrystalline pyrope ($Mg_3Al_2Si_3O_{12}$) to 9 GPa and 1000 C. Physics of The Earth and Planetary Interiors 155, 179 – 190.

Heinemann, S., Sharp, T. G., Seifert, F., Rubie, D. C., 1997. The cubic-tetragonal phase transition in the system majorite ($Mg_4Si_4O_{12}$) – pyrope ($Mg_3Al_2Si_3O_{12}$), and garnet symmetry in the Earth's transition zone. Physics and Chemistry of Minerals 24 (3), 206 – 221.

Hill, A. V., 1910. The possible effects of aggregation of the molecules of haemoglobin on its dissociation curve. Journal of Physiology 40, 4 – 7.

Hunt, S. A., Weidner, D. J., Li, L., Wang, L., Walte, N., Brodholt, J. P., Dobson, D. P., 2009. Weakening of $CaIrO_3$ during the perovskite-post perovskite transformation. Nature Geoscience, 10.1038/NGEO663.

Karato, S., Wang, Z., Liu, B., Fujino, K., 1995. Plastic deformation of garnets: systematics and implications for the rheology of the mantle transition zone. Earth and Planetary Science Letters 130 (1), 13 – 30.

Kavner, A., Sinogeikin, S. V., Jeanloz, R., Bass, J., 2000. Equation of state and strength of natural majorite. Journal of Geophysical Research 105 (3), 5963.

Leger, J. M., Redon, A. M., Chateau, C., 1990. Compressions of synthetic pyrope, spessartine and uvaorite garnets up to 25 GPa. Physics and Chemistry of Minerals 17, 161 – 167.

Leitner, B. J., Weidner, D. J., Liebermann, R. C., 1980. Elasticity of single crystal pyrope and implications for garnet solid solution series. Physics of The Earth and Planetary Interiors 22, 111 – 121.

Li, L., Long, H., Raterron, P., Weidner, D. J., 2006. Plastic flow of pyrope at mantle pressure and temperature. American Mineralogist 91, 517 – 525.

Li, L., Raterron, P., Weidner, D. J., Chen, J., 2003. Olivine flow mechansims at 8 GPa. Physics of The Earth and Planetary Interiors 138, 113 – 129.

Lui, J., Chen, G., Gwanmesia, G. D., Liebermann, R. C., 2000. Elastic wave velocities of pyrope–majorite garnets ($Py_{62}Mj_{38}$ and $Py_{50}Mj_{50}$) to 9 GPa. Physics of The Earth and Planetary Interiors 120, 153 – 163.

Nye, J. F., 1985. Physical Properties of Crystals: their Representation by Tensors and Matrices, 2nd Edition. Oxford University Press, Oxford.

O'Neill, B., Bass, J. D., Rossman, G. R., Geiger, C. A., Langer, K., 1991. Elastic properties of pyrope. Physics and Chemistry of Minerals 17, 617 – 621.

Pacalo, R. E. G., Weidner, D. J., 1997. Elasticity of majorite, $MgSiO_3$, tetragonal garnet. Physics of The Earth and Planetary Interiors 99, 145 – 154.

Poirier, J. P., 2000. Introduction to the Physics of the Earth's Interior. Cambridge Universtiy Press, Cambridge.

Rigden, S. M., Gwanmesia, G. D., Liebermann, R. C., 1994. Elastic wave velocities of a pyrope-majorite garnet to 3 GPa. Physics of The Earth and Planetary Interiors 86, 35 – 44.

Ringwood, A. E., 1991. Phase transformations and their bearing on the constitution and dynamics of the mantle. Geochimica et Cosmochimica Acta 55, 2083 – 2110.

Sato, Y., Akaogi, M., Akimoto, S., 1978. Hydrostatic compression of the synthetic garnets pyrope and almandine. Journal of Geophysical Research 83, 335 – 338.

Sinogeikin, S. V., Bass, J. D., 2002a. Elasticity of majorite and a majorite-pyrope solid solution to high pressure: Implications for the transition zone. Geophysical Research Letters 29 (2), 1017 – 1021.

Sinogeikin, S. V., Bass, J. D., 2002b. Elasticity of pyrope and majorite-pyrope solid solutions to high temperatures. Earth and Planetary Science Letters 203, 549 – 555.

Sinogeikin, S. V., Bass, J. D., O'Neill, B., Gasparik, T., 1997. Elasticity of tetragonal end-member majorite and solid solutions in the system $Mg_4Si_4O_{12}$–$Mg_3Al_2Si_3O_{12}$. Physics and Chemistry of Minerals 24, 115 – 121.

Sumino, Y., Anderson, D. L., 1984. Elastic Constants of Minerals. In: Carmichael, R. S. (Ed.), Handbook of Pyhsical Properties of Rocks. Vol. 3. CRC Press, Boca Raton, Florida, pp. 39 – 137.

van Keken, P. E., Karato, S., Yuen, D. A., 1996. Rheological control of oceanic crust separation in the transition zone. Geophysical Research Letters 23 (14), 1821 – 1824.

Vaughan, M., Weidner, D. J., Wang, Y., Chen, J. H., Koleda, C. C., Getting, I. C., 1998. T-cup: A new high-pressure apparatus for X-ray studies. Review of High Pressure Science and Technology 7, 1520 – 1522.

Voegelé, V., Ando, J. I., Cordier, P., Liebermann, R. C., 1998a. Plastic deformation of silicate garnets I. high-pressure experiments. Physics of The Earth and Planetary Interiors 108, 305.

Voegelé, V., Cordier, P., Sutter, V., Sharp, T. G., Lardeaux, J. M., Marques, F. O., 1998b. Plastic deformation of silicate garnets II. deformation microstructures in natural samples. Physics of The Earth and Planetary Interiors 108, 319.

Wang, Y., Durham, B., Getting, I. C., Weidner, D. J., 2003. The deformation-DIA: A new apparatus for high temperature triaxial deformation to pressures up to 15 GPa. Review of Scientific Instruments 74 (6), 3002 – 3011.

Wang, Y., Weidner, D. J., Zhang, J., Gwanmesia, G., Liebermann, R. C., 1998. Thermal equation of state of garnets along the pyrope-majorite join. Physics of The Earth and Planetary Interiors 105 (1-2), 59.

Wang, Z., Ji, S., 2001. Elasticity of polycrystalline silicate garnets to pressure up to 3.0 GPa. American Mineralogist 86, 1209 – 1218.

Wang, Z., Shaocheng, J., 2000. Diffusion creep in fine-grained garnetite: implications for the flow strength of subducting slabs. Geophysical Research Letters 27, 2333.

Weidner, D. J., Chen, J., Xu, Y., Wu, Y., Vaughan, M. T., Li, L., 2001. Subduction zone rheology. Physics of The Earth and Planetary Interiors 127, 67 – 81.

Weidner, D. J., Vaughan, M. T., Wang, Y., Leinenweber, K., Liu, X., Yeganeh-Haeri, A., Pacalo, R. E., Zhao, Y., 1992. Large volume high pressure research using the wiggler port at NSLS. High Pressure Research 8 (5), 617 – 623.

Yardley, B. W. D., 1977. An emperical study of diffusion in garnet. American Mineralogist 62, 793 – 800.

Yeganeh-Haeri, A., Weidner, D. J., Ito, E., 1990. Elastic properties of the pyrope-majorite solid solution series. Geophysical Research Letters 17 (12), 2453 – 2456.

Zhang, L. H., Ahsbahs, A., Geiger, C. A., 1999. Single-srystal hydrostatic compression of synthetic pyrope, almandine, spessartine, grossular and andradite garnets at high pressures. Physics and Chemistry of Minerals 27, 52 – 58.